1	Bridging the polarimetric structure and lightning activity of an isolated
2	thunderstorm cells during the cloud life cycle
3	Chuanhong Zhao, <sup>1,2</sup> * Yijun Zhang, <sup>1,3</sup> * Huiyan Zhai, <sup>2</sup> Zhe Li, <sup>1</sup> Dong Zheng, <sup>4</sup> Xueyan Peng, <sup>2</sup> Wen
4	Yao, <sup>4</sup> Sai Du, <sup>5</sup> Yuanmou Du, <sup>6</sup>
5	Affiliations
6	<sup>1</sup> Department of Atmospheric and Oceanic Sciences & Institute of Atmospheric Sciences, Fudan
7	University, Shanghai, 200438, China.
8	<sup>2</sup> Plateau Atmosphere and Environment Key Laboratory of Sichuan Province, School of Atmospheric
9	Sciences, Chengdu University of Information Technology, Chengdu, 610225, China.
10	<sup>3</sup> Shanghai Key Laboratory of Ocean-land-atmosphere Boundary Dynamics and Climate Change &
11	Shanghai Frontiers Science Center of Atmosphere-Ocean Interaction, Fudan University, Shanghai,
12	200438, China.
13	<sup>4</sup> State Key Laboratory of Severe Weather, Chinese Academy of Meteorological Sciences &
14	Laboratory of Lightning Physics and Protection Engineering, Chinese Academy of Meteorological
15	Sciences, Beijing, 100081, China.
16	<sup>5</sup> Guangdong Meteorological Service, Guangzhou, 510080, China.
17	<sup>6</sup> Beijing Weather Modification Center, Beijing, 100089, China.
18	
19	
20	
21	
22	
23	Corresponding authors: Dr. Yijun Zhang & Dr. Chuanhong Zhao are the co-corresponding authors.
24	E-mail: <u>zhangyijun@fudan.edu.cn</u> ; <u>zch@cuit.edu.cn</u>
25	
26	
27	
28	
29	

#### Abstract

30

31

32

33

34

35

36

37

38

39

40

41

42

43

44

45

46

47

48

49

50

51

52

53

54

55

56

57

58

Polarimetric structures detected by radar can characterize Ecloud microphysics and dynamics. produce lightning flashes, which can be detected as polarimetric structures by radar. Many studies have indicated that differential reflectivity (Z<sub>DR</sub>) and specific differential phase (K<sub>DP</sub>) columns, which serve as proxies for updraft strength, are related to lightning activity; moreover, the quantities of ice and supercooled liquid water strongly influence the occurrence of lightning flashes via noninductive charging. However, few studies have focused on clarifying the sequence or interactions among these factors with dynamics and microphysics from the perspective of the cloud life cycle are uncertain. Here, we improve establish the '3D mapping columns' method to identify and quantify the Z<sub>DR</sub>/K<sub>DP</sub> columns, which is based on the Cartesian grid datasets; this method is sensitive for identifying and quantifying the  $Z_{DR}$  columns in the early phase of cloud formation. Our study bridges the polarimetric structure and lightning activity within fifteenan isolated thunderstorms during the cloud life cycle. The results indicate that microphysical variations in supercooled liquid water and graupel yield better correlation coefficients for the lightning activity prediction at short warning times (e.g., 6 minutes) than dynamical variations in the Z<sub>DR</sub> column volume do; however, the trend of the Z<sub>DR</sub> column volume implies good performance at longer warning times (e.g., 12 minutes). The K<sub>DP</sub> column is likely absent in the early phase of convection development; however, it will occur in the later stage with heavily cold cloud processes, replacing the Z<sub>DR</sub> column to indicate updrafts within the reflectivity core when obvious graupels and hailstones occur. Our study improves the understanding of the polarimetric structure, which is related to dynamics and microphysics, and is also associated with lightning activity.i) the parameter most relevant to total flashes/cloud to ground flashes is the content of supercooled rainwater/graupel. ii) The onset of the Z<sub>DR</sub> column can be used to forecast lightning initiation in advance. iii) The signatures of the ZDR and KDP columns should be complementary and used to retrieve dynamic information instead of lightning activity. Notably, the variation in the Z<sub>H</sub> intensity within  $Z_{DR}$  columns has high potential for predicting lightning activity during the cloud life cycle, which is valuable for exploration in the future. Our study improves the overall understanding of cloud microphysics and lightning activity, and suggestions for using these multiple polarimetric signatures to forecast severe weather are provided.

#### Short summary

Lightning activity is highly related to the signatures of polarimetric radar on the basis of cloud electrification physics. However, few studies have focused on bridging the polarimetric structure and lightning activity during the cloud life cycle. Here, we evaluated the sequence and interactions of polarimetric parameters for indicating lightning activity from the perspective of the cloud life cycle, and the cloud microphysics of the polarimetric structure werewas explored.

Keywords: thunderstorm; lightning activity; cloud microphysics; polarimetric radar

## 1.Introduction

Lightning is a traditional indication of severe weather (e.g., tornado, hail, microbursts, etc.). Trends in lightning activity are useful for determining the severity of a thunderstorm (e.g., Gatlin and Goodman, 2010; Goodman, et al., 2005; Williams, et al., 1999; Zhang et al., 2009). Lightning activity is the electrical response to dynamic conditions (updraft or turbulence) and cloud microphysics during storm evolution, which is supported by both theoretical and field observational studies of dynamics, microphysics and lightning activity (lightning initiation or total lightning flash rate) (e.g., Baker, et al., 1999; Baker, et al., 1995; Carey and Rutledge, 2000; Mitzeva and Saunders, 1990; Souza and Bruning, 2021; Williams, et al., 1989; Zhang et al., 2004a; Zhao, et al., 2021a). Notably, many studies have focused on the relationship between lightning activity and cloud updraft or microphysics (e.g., Carey and Rutledge, 1996, 2000; Deierling and Petersen, 2008; Lang and Rutledge, 2011; López and Aubagnac, 1997; Sharma, et al., 2024; Sharma, et al., 2021).

Polarimetric radar can provide observations to improve our understanding of the coupling between convective dynamics and storm microphysics (e.g., Sharma, et al., 2024). Lightning location technology can be used to monitor the occurrence of lightning flashes in real time (e.g., Rison, et al., 1999). In this way, radar and lightning observations can be used to link cloud updrafts and microphysics with lightning activity.

Carey and Rutledge (2000) utilized a C-band polarimetric radar to study the relationship between precipitation and lightning during tropical island convection events; their results indicated that lightning activity and the surface electric field are strongly correlated with the mixed-phase ice mass and rainfall properties during the mature phase of convection. Cloud-to-ground (CG) lightning was associated with the production and subsequent descent of graupel and frozen drops from the

-10 to −20°C region; moreover, peaks in the CG lightning flash rate typically lagged behind peaks in the graupel mass aloft (Carey and Rutledge, 2000). This observational phenomenon reflects the noninductive charging between ice-phase hydrometeors, mainly graupel and ice crystals (e.g., Latham and Dye, 1989; Reynolds, et al., 1957; Saunders, 2008; Takahashi, 1978).

Before the formation of ice particles (e.g., graupel), the supercooled raindrops present in the mixed-phase zone throughout the developing and mature phases play crucial roles in storm kinematics, microphysics, and electrification. During freezing, supercooled raindrops likely provide (i) an instantaneous and abundant supply of millimetre-sized ice, (ii) a potential source of secondary ice particles, and (iii) an invigoration in the updraft due to the latent heat of freezing (Carey and Rutledge, 2000; Rosenfeld, et al., 2008; Zhao, et al., 2024; Zhao, et al., 2022). Moreover, millimetre-sized ice and secondary ice particles contribute to cloud electrification (Bringi, et al., 1996; Sharma, et al., 2024). The intensity of convective updrafts through the modulation of microphysical factors, the collision efficiency of ice particles, and the electrification temperature influence the charge structure of storms (Liu, et al., 2024; Marshall, et al., 1995; Qie, et al., 2000; Yan et al., 1996a, b; Zhang, et al., 2004b), the flash size (Bruning and MacGorman, 2013; Zheng and Zhang, 2021), and the associated lightning flash rate (Deierling and Petersen, 2008; Deierling, et al., 2008; Fridlind, et al., 2019; Souza and Bruning, 2021; Zhao, et al., 2021a).

Moreover, supercooled raindrops produce a differential reflectivity ( $Z_{DR}$ ) column, one of the most notable polarimetric radar signatures of convective storms. High  $Z_{DR}$  values (e.g., >1 dB) above the 0°C isotherm height (meltingfreezing level) are associated with large supercooled raindrops and wet hail suspended in deep convective updrafts (e.g., Krause and Klaus, 2024; Kumjian, et al., 2014; Snyder, et al., 2015; Zhao, et al., 2020). Depending on the intensity of the updraft, the region of high  $Z_{DR}$  can extend several kilometres above the 0°C isotherm height. This narrow vertical extension of high  $Z_{DR}$  values above the environmental 0°C level associated with updrafts in strong convective storms is called the  $Z_{DR}$  column (Krause and Klaus, 2024; Kumjian, et al., 2014; Zhao, et al., 2020).

The  $Z_{DR}$  columns, due to the vertical size sorting of drops in warm-rain precipitation processes, encompass the signals of both microphysical features and updrafts; however, these signals are not present throughout the life cycle of strong convective storms, except in the early phase of cloud

development. During the initial phase of a thunderstorm, the  $Z_{DR}$  column above the melting freezing level indicates the presence of a low concentration of large raindrops (>2 mm); in addition, the  $Z_{DR}$  column expands downwards from above due to the collision and coalescence of drops and the accretion of droplets, resulting in the formation of larger raindrops (>4–5 mm) (Kumjian, et al., 2014). During the mature phase of a thunderstorm, the  $Z_{DR}$  column above the melting freezing level may continue expanding upwards and outwards because stronger updrafts loft raindrops upwards into the mixed-phase layer, but smaller drops reach their nucleation temperature and begin to freeze while ascending to higher altitude. As these supercooled raindrops begin to freeze and mix with water-coated graupel and hail, the corresponding  $Z_{DR}$  values decrease, denoting top of the  $Z_{DR}$  column. As updrafts subsequently weaken and large ice particles (high-density graupel or hailstones) increase in abundance, the  $Z_{DR}$  column starts to collapse; however, lightning activity may exhibit an inverse trend compared with that of the  $Z_{DR}$  column at this moment. For example, as shown by Sharma et al. (2024), after the first lightning jump, the subsequent lightning jumps are associated with a decreasing trend in the  $Z_{DR}$  column volume.

On the other hand, in the specific differential phase (K<sub>DP</sub>) column, high values (>0.75°/km, the value reported by Loney et al. (2002)) above the meltingfreezing level occur and are strongly associated with a high concentration of water-coated ice (e.g., water-coated graupel and hail with a non-spherical shape) and raindrops (1–2 mm) that shed from hailstones growing in a wet regime (Bringi, et al., 1996; Hubbert, et al., 1998; Loney, et al., 2002). Thus, the formation of a K<sub>DP</sub> column is tied to cold cloud microphysics, which usually lagoceurring behind the appearance of the Z<sub>DR</sub> column.later in the life cycle of a thunderstorm.

van Lier-Walqui et al. (2016) attempted to <u>constraindetermine the constraints of</u> cloud-resolving models on the basis of ground-based remote sensing observations, namely, polarimetric radar data. In their study, the K<sub>DP</sub> column (specifically, the column volume) was strongly related to the updraft mass flux, lightning activity, and rainfall intensity in four deep convection events observed during the Midlatitude Continental Convective Clouds Experiment. Recently, Sharma et al. (2024) utilized polarimetric radar observations of three severe storms during the VORTEX-Southeast field campaign to quantify the correlation between the volumes of Z<sub>DR</sub> and K<sub>DP</sub> columns (representative of mixed-phase microphysics as well as updraft intensity and size) and total lightning

flash rates. They indicated that the volume of the K<sub>DP</sub> columns exhibited high co-variability with the total flash rate in three such cases (a tornadic supercell embedded in a stratiform precipitation system, a non-tornadic supercell, and a supercell embedded within a quasilinear convective system). Sharma et al. (2024) conducted a study on the basis of hypotheses, namely, that the deeper and wider the Z<sub>DR</sub> and K<sub>DP</sub> columns were in cases with robust and wide updrafts (e.g., Homeyer and Kumjian, 2015; Snyder, et al., 2017), the more an increase in the volumes of the Z<sub>DR</sub> and K<sub>DP</sub> columns would correspond to an increase the mixed-phase ice mass flux, resulting in an increase in the total flash rate; therefore, the correlation coefficient (-0.47~0.37 for the Z<sub>DR</sub> column; 0.54~0.74 for the K<sub>DP</sub> column) between Z<sub>DR</sub> or K<sub>DP</sub> columns and lightning activity was not as high as the microphysical parameters explored in previous studies (e.g., Carey and Rutledge 2000). Moreover, the results seem to be inconsistent with those of Sharma et al. (2021), who reported that the variability in flash rates is best explained by fluctuations in the Z<sub>DR</sub> column volume, with a high correlation coefficient value (0.72). In addition, tOne possible explanation is that the effect of the time lag may decrease this correlation coefficient. As reported by Carey and Rutledge (2000), they obtained a very high one-lag (7 minutes) correlation coefficient ( $\rho = 0.9$ ) between the graupel mass within the mixed-phase zone and the CG lightning flash rate, suggesting that the directly related microphysics with noninductive charging have a greater correlation coefficient with lightning activity. Another possible way is that the interactions of the  $Z_{DR}/K_{DP}$  column with dynamics and microphysics are uncertain, which affects the results under the current hypotheses. This is also emphasized in Sharma et al. (2021) and raised as a retained question in the appendix. Thus, further exploration is needed.

147

148

149

150

151

152

153

154

155

156

157

158

159

160

161

162

163

164

165

166

167

168

169

170

171

172

173

174

175

In summary, <u>four parameters dynamical and microphysical characteristics</u> derived from polarimetric radar can provide forecasting information about lightning activity on the basis of noninductive charging: i) the precipitation-sized (e.g., graupel) ice mass within the mixed-phase zone; ii) the content of supercooled raindrops; and iii) the quantified Z<sub>DR</sub> and K<sub>DP</sub> columns (e.g., the column volume or height). Our goal in this study is to link these <u>four polarimetric radar variables parameters</u> for forecasting lightning activity within isolated thunderstorm cells during the cloud life cycle over South China, <u>determine of whether the best proxy among these four parameters is used to forecast lightning activity, and and determine how the cloud microphysics <u>and dynamics</u></u>

related to these <u>polarimetric radar variables</u> four <u>parameters</u> should be assessed. Notably, the close relationship between these <u>polarimetric radar variables</u> four <u>parameters</u> and lightning activity has been noted in many studies (e.g., Carey and Rutledge, 2000; Hayashi et al., 2021; Sharma et al., 2024; Sharma, et al., 2021; Snyder, et al., 2015; van Lier-Walqui, et al., 2016; Woodard et al., 2012); thus, we believe that this study is sufficient for connecting these <u>polarimetric radar variables</u> four <u>parameters</u> and lightning activity via <u>an</u> the anatomy of an isolated <u>thunder</u>storm cell during the cloud life cycle <u>and the statistical results of fifteen isolated thunderstorm cells</u>.

This paper is organized as follows. In Section 2, an overview of the radar and lightning data is given, and the analysis methods and the approach for quantifying the  $Z_{DR}/K_{DP}$  columns are described. Section 3 presents the results of  $Z_{DR}/K_{DP}$  column quantification and the related characteristics of the polarimetric structure and microphysics with the  $Z_{DR}/K_{DP}$  column. The vertical structures of polarimetric radar variables and microphysics are explored in combination with 3D lightning location data, and the microphysical characteristics of the  $Z_{DR}$  column; additionally, the variation in the ice/water content within the mixed phase zone with cloud development is illustrated, and the The relationship between lightning activity and these polarimetric characteristics in cases and statistics is presented. Finally, we summarize the results in Section 4.

#### 2.Data and methodology

#### 2.1. Radar and lightning observations

This study included 15 isolated thunderstorm cells that produced lightning, which was observed via an S-band dual-polarization radar deployed in Guangzhou city (GZ radar) and a low-frequency E-field detection array (LFEDA) (Table 1). The average 6-hourly convective available potential energy (CAPE) of these thunderstorms was obtained from ERA-Interim reanalysis data, as in Zhao et al. (2022). The detailed examination of lightning activity with related dynamics and microphysics in case #1 was conducted first, and then the statistical results of all cases were given. On 20 June 2016, one isolated thunderstorm cell was observed by the GZ radarvia an S-band dual-polarization radar deployed in Guangzhou city (GZ radar) (Figure 1). The composite reflectivity data revealed that this thunderstorm (the boundary was determined via manual inspection; the black lines in Figure 1) was nearly stationary and that the cloud life cycle lasted approximately two hours. Lightning activity occurred when values of composite reflectivity >35 dBZ were present; this

phenomenon seemingly supported the results of Hayashi et al. (2021), highlighting the importance of graupel in cloud electrification.

Table 1. The information of cases

Cases number	Time information [CST]	CAPE [J kg <sup>-1</sup> ]
<u>#1</u>	17:18 to 19:00, 20 June 2016	<u>1277</u>
<u>#2</u>	12:12 to 13:18, 26 June 2016	<u>1225</u>
<u>#3</u>	15:36 to 16:36, 3 July 2016	<u>961</u>
<u>#4</u>	16:06 to 17:06, 5 July 2016	<u>412</u>
<u>#5</u>	11:00 to 12:12, 6 July 2016	<u>1202</u>
<u>#6</u>	16:18 to 17:06, 6 July 2016	<u>1202</u>
<u>#7</u>	15:00 to 16:06, 16 July 2016	<u>1425</u>
<u>#8</u>	13:24 to 14:12, 27 July 2016	<u>1203</u>
<u>#9</u>	14:36 to 15:18, 27 July 2016	<u>1376</u>
<u>#10</u>	14:54 to 15:18, 27 July 2016	<u>1286</u>
<u>#11</u>	13:24 to 15:00, 29 May 2016	<u>1339</u>
<u>#12</u>	09:18 to 10:48, 18 June 2016	<u>1437</u>
<u>#13</u>	12:18 to 13:00, 18 June 2016	<u>1375</u>
<u>#14</u>	15:48 to 16:36, 18 June 2016	<u>1475</u>
<u>#15</u>	13:06 to 14:12, 7 July 2016	<u>2537</u>

The beam width of the GZ radar is  $\leq 1^{\circ}$ , and the azimuth and range resolutions are  $1^{\circ}$  and 250 m, respectively. A full radar volume scan lasted 6 minutes at nine elevation angles. The GZ radar data were processed via the Python ARM Radar Toolkit (Py-ART), including quality control (Helmus and Collis, 2016; Li, et al., 2023; Li, et al., 2024). The  $Z_{DR}$  offset of the raw data was corrected via drizzle, and the calibration accuracy was expected to be 0.1–0.2 dB (Bringi and Chandrasekar, 2001). We utilized two methods to smooth the differential phase  $\Phi_{DP}$ , namely, "lightly filtering" (2-km) and "heavily filtering" (6-km), as in Park et al. (2009). Two estimates of  $K_{DP}$  were subsequently obtained from a slope of a least squares fit of the filtered  $\Phi_{DP}$ ; a lightly filtered  $K_{DP}$  was subsequently used in the case of horizontal reflectivity  $\geq$  40 dBZ, and a heavily filtered  $K_{DP}$  was selected otherwise (Ryzhkov and Zrnić, 1996). The radar data were gridded via Py-ART gridding routines on a Cartesian grid with a 0.25-km horizontal resolution and a 500-m vertical resolution ("Barnes2" method).

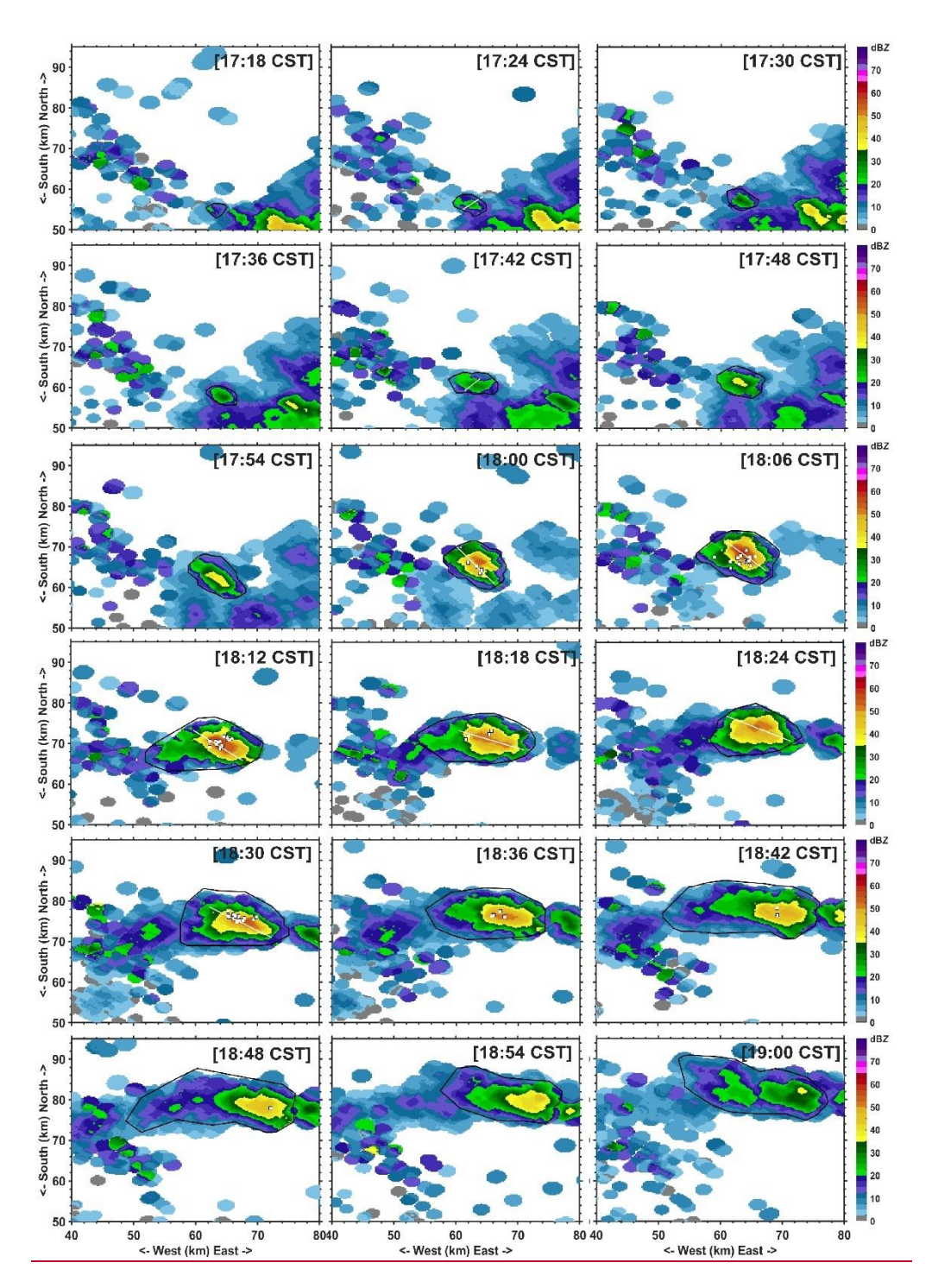


Figure 1. The composite reflectivity of the isolated thunderstorm cell on 20 June 2016 (case #1), which initiated at 17:18 and ended at 19:00 (China Standard Time, CST). The black lines indicate the boundary of this thunderstorm.

The white squares (intracloud flashes) and triangles (CG flashes) black crosses indicate the lightning flashes, and the location of once lightning flash is represented by the location of the first discharge pulse event. The positions for the plotted cross section are shown as white lines over the composite reflectivity data.

The lightning flashes within this thundercloud were detected via a low frequency E field detection array (LFEDA), which is a 3-D mapping detection system for intracloud and CG lightning, with 10 sensors. Previous studies (Fan, et al., 2018; Shi, et al., 2017) utilized information from triggered lightning flashes to evaluate LFEDA detection results; the results show the detection efficiency of the LFEDA can reach 100%, and the mean location error is 102 m. Discharge pulse events were grouped into a lightning flash via the same method as described by Liu et al. (2020). A potential discharge pulse event of one lightning flash should occur within 0.4 s of the previous discharge pulse event and within 0.6 s and 4 km of any other discharge pulse event of this lightning flash. If any source within one lightning flash is below the 2-km height, this lightning flash iswas regarded as one cloud-to-ground flash, as suggested by Zhao et al. (2021a).

The lightning flashes were assigned to the isolated thunderstorm on the basis of the boundary of the thunderstorm, as well as a constraint every 6 minutes (according to the duration of a full radar volume scan). The life cycle of this isolated thunderstorm initiated from the first radar echo (i.e., the presence of a maximum horizontal reflectivity  $(Z_H) \ge 5$  dBZ in a full radar volume scan within this cloud was first detected by the GZ radar, as suggested by Zhao et al. (2021a, 2022, 2024)) and ended when the maximum  $Z_H$  started to decrease and the  $Z_H$  reached  $\le 40$  dBZ. The distributions of these detection systems, including radar and lightning location system, were illustrated by in Zhao et al. (2024).

## 2.2. Cloud microphysical parameter retrieval methods

To estimate the precipitation-sized ice mass (e.g., graupel, hail, and frozen drops) and the content of supercooled raindrops within the mixed-phase zone, an approach on the basis of difference reflectivity ( $Z_{DP}$ , dB) is applied (Carey and Rutledge, 2000; Straka et al., 2000).

$$Z_{h} = (4\lambda^{4}/\pi^{4}|K_{w}|^{2})\langle|S_{hh}|^{2}\rangle \tag{1}$$

$$Z_{\nu} = (4\lambda^{4}/\pi^{4}|K_{w}|^{2})\langle|S_{\nu\nu}|^{2}\rangle$$
 (2)

$$Z_{\rm DP} = 10 \log_{10}(Z_h - Z_v), \text{ for } Z_h > Z_v$$
 (3)

 $S_{ij}$  refers to an element of the backscattering matrix of a hydrometeor (Zrnić, 1991). The first subscript i indicates the polarization of the backscattered field (h is horizontal, v is vertical), and the second subscript j indicates the polarization of the incident field.  $K_w=(\epsilon_w-1)/(\epsilon_w+2)$  is the factor associated with the dielectric constant of water, and  $\epsilon_w$  is the dielectric constant.  $\lambda$  is the radar

wavelength. The brackets indicate expectations expressed in terms of the distribution of mean hydrometeor properties such as shape, size, fall orientation, particle density, canting angle, dielectric constant, and others.

Pruppacher and Klett (1997) assumed that precipitation-sized ice particles were more spherically symmetrical or tumble. The low dielectric constant and significant canting behaviour of ice particles likely result in a near-zero  $Z_{DR}$  (e.g., Seliga and Bringi, 1976). Therefore, the horizontal reflectivity and vertical reflectivity are equal for ice particles, as "effective spheres", and  $Z_{DP}$  is solely influenced by raindrops. If the relationship between horizontal reflectivity and  $Z_{DP}$  (raindrops) is known, the horizontal reflectivity of raindrops can be derived. The relationship between the horizontal reflectivity of raindrops and  $Z_{DP}$  (raindrops) is derived from 2-year disdrometer data in Guangdong Province (Li et al., 2019), which is suitable for the current radar used in this study:

$$Z_{H}^{rain} = 0.0044 Z_{DP}^{2} + 0.58054 Z_{DP} + 16.591$$
 (4)

Then, the ice echo intensity  $Z_{\rm H}^{\rm ice}$  can be expressed as  $Z_{\rm H}-Z_{\rm H}^{\rm rain}$ . The standard error for the relationship between horizontal reflectivity and  $Z_{\rm DP}$  is consistently approximately 1 dB (Carey and Rutledge, 2000). If  $Z_{\rm H}-Z_{\rm H}^{\rm rain}<1$  dB, which is below the melting layer,  $Z_h^{\rm ice}=0$  mm<sup>6</sup>m<sup>-3</sup>,  $Z_{\rm H}^{\rm rain}=10\log_{10}(Z_h^{\rm rain})$ , and  $Z_h^{\rm rain}=Z_h$ . In contrast, above the melting layer, if  $Z_{\rm H}-Z_{\rm H}^{\rm ice}<1$  dB, then  $Z_h^{\rm rain}=0$  mm<sup>6</sup>m<sup>-3</sup>, and  $Z_h^{\rm ice}=Z_h$  (Carey and Rutledge, 2000). The estimates of rain mass ( $M_{\rm w}$ , g m<sup>-3</sup>) and ice mass ( $M_{\rm ice}$ , g m<sup>-3</sup>) are derived via the following reflectivity–mass relationships (Chang et al., 2015; Zhao et al., 2022):

$$M_w = 3.44 \times 10^{-3} \left( Z_h^{rain} \right)^{4/7}$$
 (5)

$$M_i = 1000\pi \rho_i N_0^{3/7} \left( \frac{5.28 \times 10^{-18} Z_h^{ice}}{720} \right)^{4/7}$$
 (6)

where  $\rho_i$  indicates the ice density (kg m<sup>-3</sup>),  $N_0$ =4×10<sup>6</sup> m<sup>-4</sup>. The estimated ice mass from the horizontal reflectivity of ice particles is proportional to the actual ice mass and depends on the variability in the intercept parameter of an assumed inverse exponential distribution for ice and the ice density; thus, the trends of the estimated ice mass are deemed sufficient to investigate lightning activity. Importantly, the  $Z_{DP}$  can differentiate between ice and rain only if the  $Z_H$  is sufficiently large (i.e., diameter  $\geq$  1 mm); under such conditions, the raindrop is characterized by significant oblateness (Carey and Rutledge, 2000; Green, 1975).

The estimated ice masses are assigned to graupel masses on the basis of scattering properties, namely, where the Z<sub>H</sub> values exceed 35 dBZ (Carey and Rutledge, 2000; Kumjian, 2013a, b; Zhao, et al., 2021b). The threshold value is usually applied to identify graupel in hydrometeor identification method (Park et al., 2009). (Carey and Rutledge, 2000; Kumjian, 2013a, b; Zhao, et al., 2021b). The rain water content above the meltingfreezing level (0°C isotherm height; sounding data from the Qingyuan meteorological observatory are used to obtain the environmental temperature) is defined as the supercooled raindrop mass.

 $Z_{DR}$  columns are associated with low concentration of large raindrops (>2 mm); thus, the median volume diameter  $D_0$  of raindrops is retrieved via the method described by Hu and Ryzhkov (2022) to provide supporting evidence for identifying  $Z_{DR}$  columns. Notably,  $D_0$  is not used to identify  $Z_{DR}$  columns directly but rather to ensure the threshold value of  $Z_{DR}$ , which is utilized to identify  $Z_{DR}$  columns directly. The fractional standard deviation of the  $D_0$  estimation is approximately 10% (Hu and Ryzhkov, 2022).

To further explore the characteristics of the microphysics related to the  $Z_{DR}/K_{DP}$  column and lightning within these thunderstorms, hydrometeor identification method involving the fuzzy-logic algorithm (as in Zhao et al., 2021b) and the microphysical fingerprint (following Kumjian et al., 2022) are conducted. Identifying polarimetric radar "fingerprints" of ongoing microphysical processes was introduced by Kumjian (2012); these fingerprints are defined as vertical changes in two (e.g.,  $Z_H$ ,  $Z_{DR}$ ) or more of the dual-polarization radar variables (Kumjian et al., 2022).

As suggested by Kumjian et al. (2022), the co-polar correlation coefficient (CC) is neglected in most of the fingerprints discussed but it is important to indicate the melting process; thus, we added the changes in the CC towards the ground to identify the melting process. The changes in the polarimetric radar variables towards the ground for riming and aggregation are the same (Kumjian et al., 2022); however, the riming process is valuable for studying lightning activity. Thus, we followed the method for identifying the aggregation and graupel particles in Park et al. (2009), namely, we utilized the discriminated convective and stratiform echoes to determine where riming or aggregation processes occur. If the echo is classified as convective, then the aggregation process is not allowed within a whole vertical column; conversely, the riming process is excluded in the stratiform case.

In addition, the 0°C isotherm height is used to discriminate warm-rain processes and mixed-phase processes; notably, this rule introduces potential errors when it is used where the  $Z_{DR}/K_{DP}$  column is used. Specifically, the polarimetric characteristics of collision-coalescence and size sorting (or evaporation) processes above the 0°C isotherm height are regarded as vapour deposition and refreezing processes, respectively. In this study, we utilize the identified and quantified  $Z_{DR}/K_{DP}$  columns to correct this possible error. A summary of the changes in the polarimetric radar variables towards the ground and additional conditions for different microphysical processes is displayed in Table 2. To characterize the microphysical fingerprints in this study, the changes in the polarimetric radar variables towards the ground are computed between two adjacent grids in the vertical direction (for example,  $\Delta Z_H$  (x, y,  $z_1$ ) =  $Z_H$  (x, y,  $z_2$ ) –  $Z_H$  (x, y,  $z_1$ ), x, y, and z are the three dimensions in the Cartesian coordinate system;  $z_1$  is 500 m in height, and  $z_2$  is 1000 m in height). The minimum thresholds of  $\Delta Z_H > 0.002$  dB/km and  $\Delta Z_{DR} > 0.0001$  dB/km are applied to avoid false classifications based on noise present in the data, as in Kumjian et al. (2022).

Table 2. Changes in the polarimetric radar variables towards the ground for different microphysical processes. An increase in that radar variable between the top and bottom of the profile is indicated by a positive sign +, whereas a decrease is indicated by a negative sign.

Microphysical processes	$\Delta Z_{\rm H}$	$\Delta Z_{DR}$	ΔCC	Convective/Stratiform area	ZDR/KDP column
Collision-Coalescence	<u>+</u>	<u>+</u>	<u>/</u>	<u>/</u>	√_
<u>Breakup</u>	Ξ	Ξ	<u>/</u>	<u>/</u>	<u>/</u>
Size Sorting/Evaporation	=	<u>+</u>	<u>/</u>	<u>/</u>	$\sqrt{}$
Vapour Deposition	<u>+</u>	<u>+</u>	<u>/</u>	<u>/</u>	×
<u>Aggregation</u>	<u>+</u>	=	<u>/</u>	Stratiform area	<u>/</u>
Riming	<u>+</u>	Ξ	<u>/</u>	Convective area	<u>/</u>
Sublimation (with	Ξ	Ξ	<u>/</u>	<u>/</u>	<u>/</u>
fragmentation)/Refreezing					
Refreezing	Ξ	<u>+</u>	<u>/</u>	<u>/</u>	×
Melting	<u>+</u>	<u>+</u>	=	<u>/</u>	<u>/</u>

### 2.3. Previous automatically identification and quantification methods for Z<sub>DR</sub>/K<sub>DP</sub> columns

Currently, a few methods are available to automatically identify and quantify  $Z_{DR}/K_{DP}$  columns (e.g., Woodard et al., 2012; Krause and Klaus, 2024; Sharma, et al., 2024; Snyder, et al., 2015; van Lier-Walqui, et al., 2016). These methods are constructed on the basis of the morphology of the  $Z_{DR}/K_{DP}$  columns and/or the high values (e.g.,  $Z_{DR} > 1$  dB;  $K_{DP} > 1^{\circ}/k_{DP}$ ) above the meltingfreezing level.

In the stage of cloud formation, high  $Z_{DR}$  values above the melting freezing level are simply used to identify  $Z_{DR}$  columns; however, these high values are not always associated with the  $Z_{DR}$  columns. Notably, three-body scatter signatures (Zrnić, 1987), depolarization streaks associated with the canting behaviour of ice in regions of strong electrification (Kumjian, 2013c), and oblate ice particles can lead to enhanced positive  $Z_{DR}$  values (Kumjian, 2013a). Thus, additional requirements were imposed to avoid identification errors, e.g., the reflectivity threshold value ( $Z_{H} \ge 40 \text{ dBZ}$ ) (Woodard et al., 2012) and the height should be below the homogeneous melting freezing level, and the maximum height of the  $Z_{DR}$  column should be associated with the height at which  $Z_{DR}$  displays a negative vertical gradient (van Lier-Walqui, et al., 2016).

Recently, Krause and Klaus (2024) utilized the hotspot technique to identify the base of the  $Z_{DR}$  column on the basis of constant altitude plan projection indicators (CAPPIs). Although their results indicated an improvement in the plan region identified on the basis of the  $Z_{DR}$  column approach over the results of two different existing algorithms (Thunderstorm Risk Estimation from Nowcasting Development via Size Sorting algorithm and the algorithm introduced by Snyder et al. (2015)), the depth and volume information for  $Z_{DR}$  columns was lost, which was not beneficial for forecasting lightning activity. In addition, the reflectivity threshold value ( $Z_{H} > 25 \text{ dBZ}$ ) was required in this algorithm. Sharma et al. (2024) used an algorithm in the "scikit-image" Python package to identify  $Z_{DR}/K_{DP}$  columns from Cartesian grid data via threshold values ( $Z_{DR} \ge 1 \text{ dB}$ ;  $K_{DP} \ge 1^{\circ}/\text{km}$ ); they restricted the  $Z_{H}$  values to exceed 20 dBZ, and any instances of obvious data contamination or unrealistic values during the gridding process were manually removed prior to analysis. They focused on three supercells during lightning activity, and violent convection in such case will ignore the formation of  $Z_{DR}/K_{DP}$  columns at weak echo intensities, i.e., in the initiation stage of convective clouds.

# 2.4. Automatic 3D mapping of $Z_{DR}/K_{DP}$ columns during the life cycle of an isolated cell storm

Our objective in this study is to explore the performance of microphysics retrieved via radar for forecasting lightning activity within isolated thunderstorm cells during the cloud life cycle. As depicted in Figure 1, our radar observations indicate that before the initiation of lightning, the echo intensity is weak during the early stage of a cloud. Moreover, we seek to determine whether  $Z_{DR}$  columns form in the early stages of cloud formation. In addition,  $K_{DP}$  columns are representative of

small drops with high concentration shed from large ice particles (e.g., hailstones) growing in a wet regime (Hubbert, et al., 1998; Loney, et al., 2002), thus, are K<sub>DP</sub> columns absent in the initial stage of convective cloud formation and even in early stages of lightning activity?

Figure 2 shows the first appearance of the  $Z_{DR}$  column at 17:24 (China Standard Time, CST), which is ~36 minutes earlier than the first lightning occurrence and only lags behind the first radar echo by 6 minutes. The high values of  $Z_{DR}$  extend to the mixed-phase region from the cloud bottom, and the height of the  $Z_{DR}$  column is approximately 1 km (Figure 2c). The corresponding  $Z_H$  values are smaller than 30 dBZ, but with the values of the co-polar correlation coefficient (CC) are relatively high (Figure 2a, d). These characteristics indicate the presence of large raindrops with low concentrations; the low  $K_{DP}$  values and large size of raindrops (exceeding 2 mm) support that (Figure 2e, f)<sub>25</sub> weWe illustrate the microphysical structure corresponding to high  $Z_{DR}$  values in Figure 2b. The threshold value for identifying the  $Z_{DR}$  column in this study is 1.5 dB, considering that the size of raindrops should exceed 2 mm within the  $Z_{DR}$  column during the initial phase of a storm (e.g., Kumjian, et al., 2014). In addition, the  $K_{DP}$  column is absent in the initial phase of this storm, not appearing until 18:30 CST.

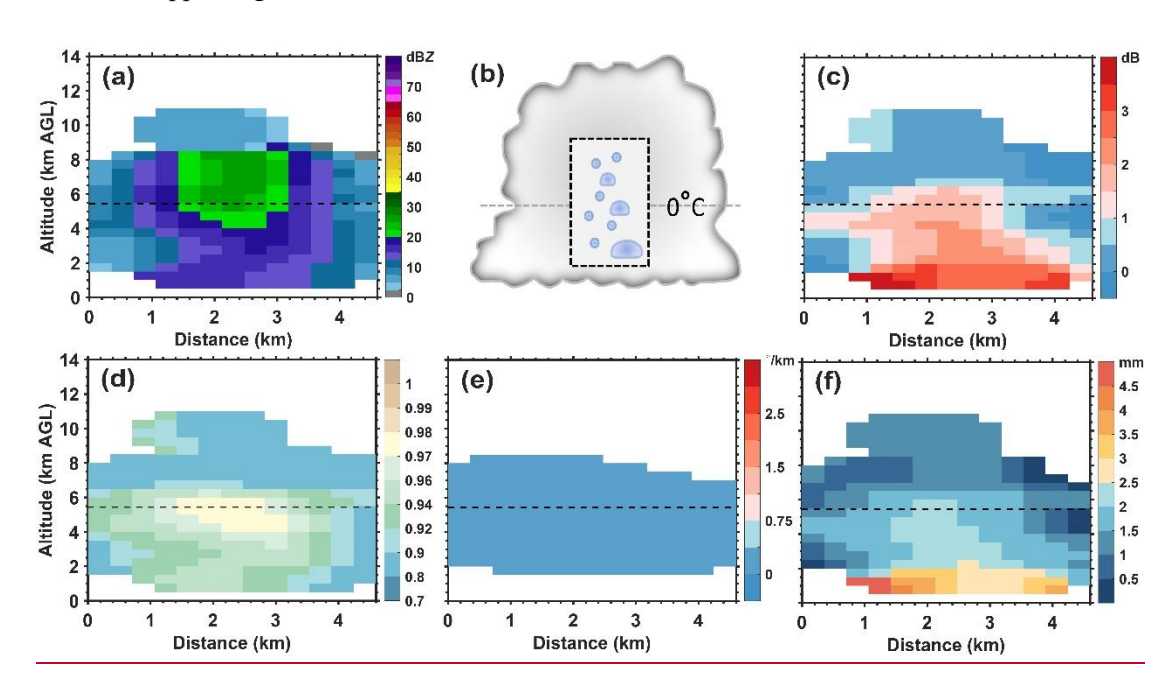


Figure 2. Cross section from the Cartesian grid of the studied isolated thunderstorm at 17:24 CST. (a)  $Z_H$ . (b) Conceptual model of the microphysical structure within high  $Z_{DR}$  values. (c)  $Z_{DR}$ , (d) CC, (e)  $K_{DP}$ . (f) Median volume diameter  $D_0$  of raindrops. The black dashed line indicates the 0°C isotherm height. AGL (above ground

In this study, we <u>improvedestablish</u> a method that only depends on the  $Z_{DR}$  parameter for identifying and easily quantifying the  $Z_{DR}$  column (e.g., height and volume) during the whole life cycle of a storm, specifically, including the initial phase of a convective cloud; the morphology of the  $Z_{DR}$  column <u>resulting from resulted by</u> size sorting and the high  $Z_{DR}$  values ( $\geq 1.5$  dB) in Cartesian grid data are combined as the basis of this method. A flow chart of this method is depicted in Figure 3.

First, we establish logic matrices with the same specifications as the  $Z_{DR}$  matrices and identify the layer that corresponds to the 0°C isotherm height (with sounding data used to determine the environmental temperature). Second, from the 1-km height below the meltingfreezing level to the mixed-phase region, if  $Z_{DR} \ge 1.5$  dB, the corresponding logic values in the logic matrix are equal to 1. Notably, we utilize the lower portion of the logic matrix to upwards restrict the possible errors associated with including locations outside the successive column of high  $Z_{DR}$  values ( $\ge 1.5$  dB). This restriction condition is based on the column morphology (columnar shape), which results from drop size sorting. Specifically, the region of the  $Z_{DR}$  column contracts upwards from the 0°C isotherm height below the mixed-phase region (e.g., as shown in Amiot et al. (2019), Hubbert et al. (2018), Kumjian et al. (2014), Snyder et al. (2015) and Tuttle et al. (1989)). In the Cartesian grid data, this phenomenon is particularly obvious (Figure 2c).

Third, the size distribution of raindrops within the  $Z_{DR}$  column is determined by size sorting; thus, we utilize the negative vertical gradient of  $Z_{DR}$  on the basis of every grid between two adjacent layers from the  $0^{\circ}C$  isotherm height to the uppermost limit height to further ensure that the grids are associated with the  $Z_{DR}$  column. Finally, a 3D mapping of the  $Z_{DR}$  column is constructed. We can use the grid information to compute the height and volume of the  $Z_{DR}$  column. Although the formation mechanism of the  $K_{DP}$  column is different from that of the  $Z_{DR}$  column, the morphology of the  $K_{DP}$  column is highly consistent with that of the  $Z_{DR}$  column; thus, this method can be applied to map the  $K_{DP}$  column with a 3D grid based on the threshold value for identifying the  $K_{DP}$  column (e.g.,  $\geq 1^{\circ}/km$ ).

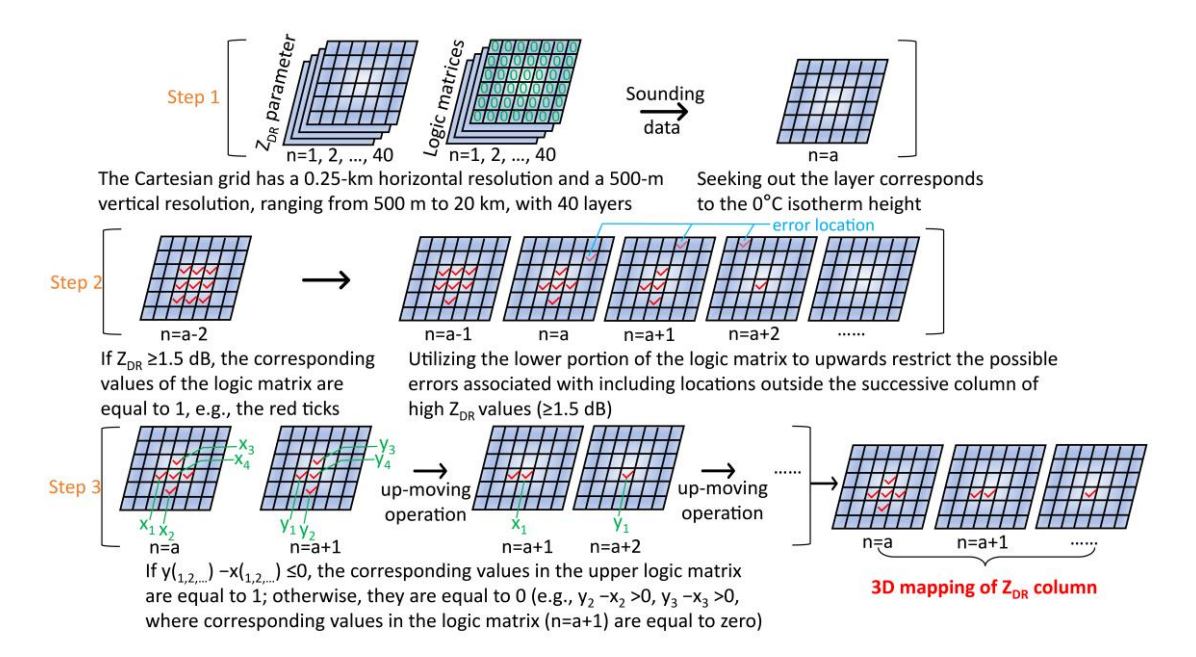


Figure 3. Flow chart of 3D mapping of a Z<sub>DR</sub> column.

## 3. Results

## 3.1. Assessment of Z<sub>DR</sub>/K<sub>DP</sub> columns identified via the "3D mapping columns" method

Snapshots of the identified  $Z_{DR}$  columns via the "3D mapping columns" method at four moments (the  $K_{DP}$  column only existed at one moment during the life cycle of this thunderstorm) are shown in Figure 4. The identified regions of the  $Z_{DR}/K_{DP}$  columns are represented by white dots. We verify that the "3D mapping columns" method performs well in identifying the  $Z_{DR}/K_{DP}$  columns via manual inspection.

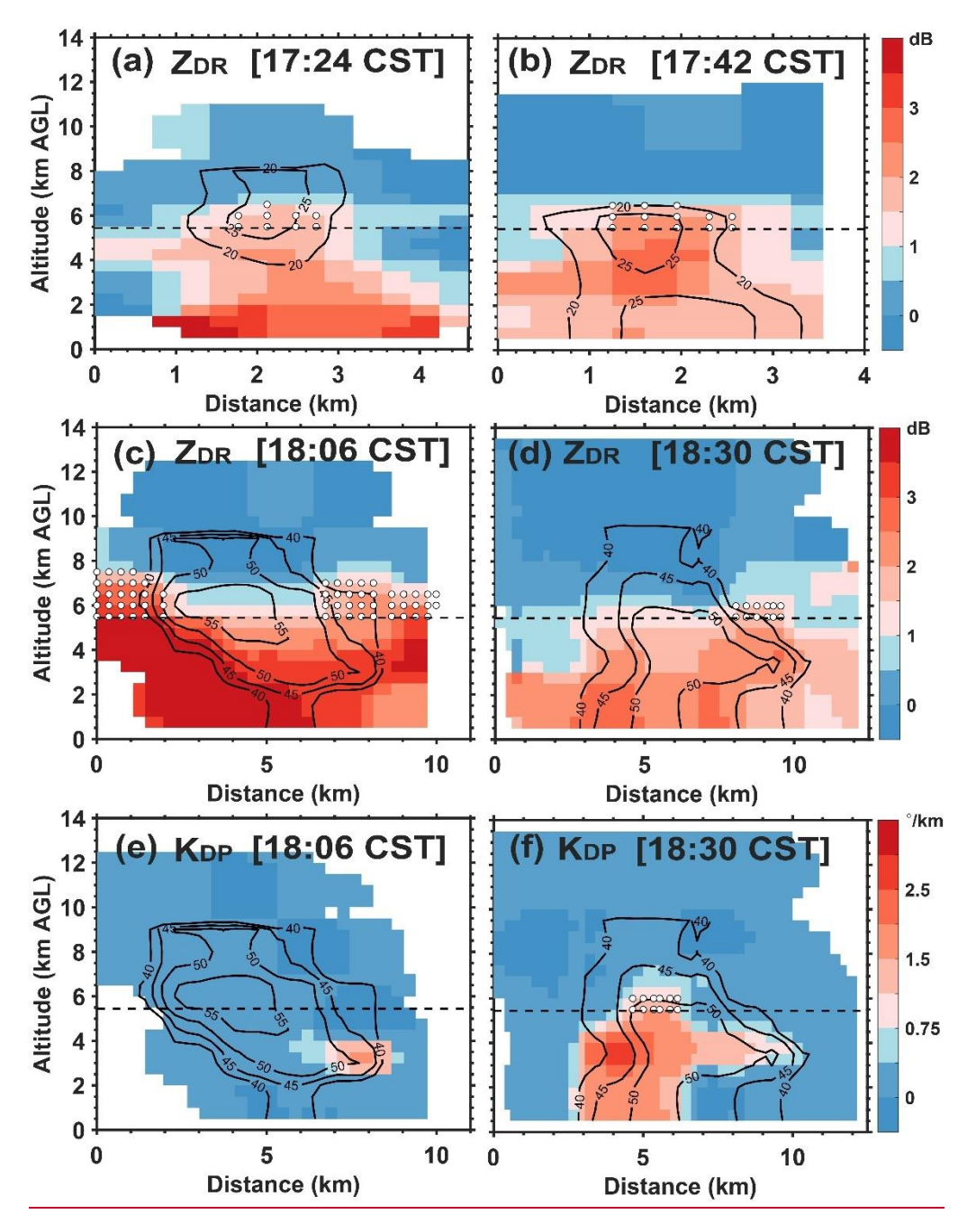


Figure 4. Cross sections from the Cartesian grid of the studied isolated thunderstorm at (a) 17:24 CST, Z<sub>DR</sub>; (b) 17:42 CST, Z<sub>DR</sub>; (c) 18:06 CST, Z<sub>DR</sub>; (d) 18:30 CST, Z<sub>DR</sub>; (e) 18:06 CST, K<sub>DP</sub>; and (f) 18:30 CST, K<sub>DP</sub>. The black dashed line indicates the 0°C isotherm height. The white dots indicate the areas of the identified Z<sub>DR</sub>/K<sub>DP</sub> columns.

The black contours with values indicate the reflectivity structure. AGL (above ground level).

The first  $Z_{DR}$  column in this isolated thunderstorm occurred at 17:24 CST (Figure 4a, Figure 5a). The second  $Z_{DR}$  column subsequently occurred at 17:42 CST after 18 minutes (Figure 4b, Figure 5a). At 18:06 CST, the lightning activity reached the first peak (Figure 65; to compare the radar and lightning data, the lightning flash frequency was counted every 6 minutes), and the  $Z_{DR}$  column was

the highest and largest (in volume) at this time (Figure 5a). However, the overlap region between the  $Z_{DR}$  column and reflectivity core at 17:24 and 17:42 CST disappeared at 18:06 CST (Figure 4c); i.e., the  $Z_{DR}$  column within the reflectivity core began to collapse because of the falling of large-sized (represented by  $Z_{H}$  values exceeding 40 dBZ) ice particles.

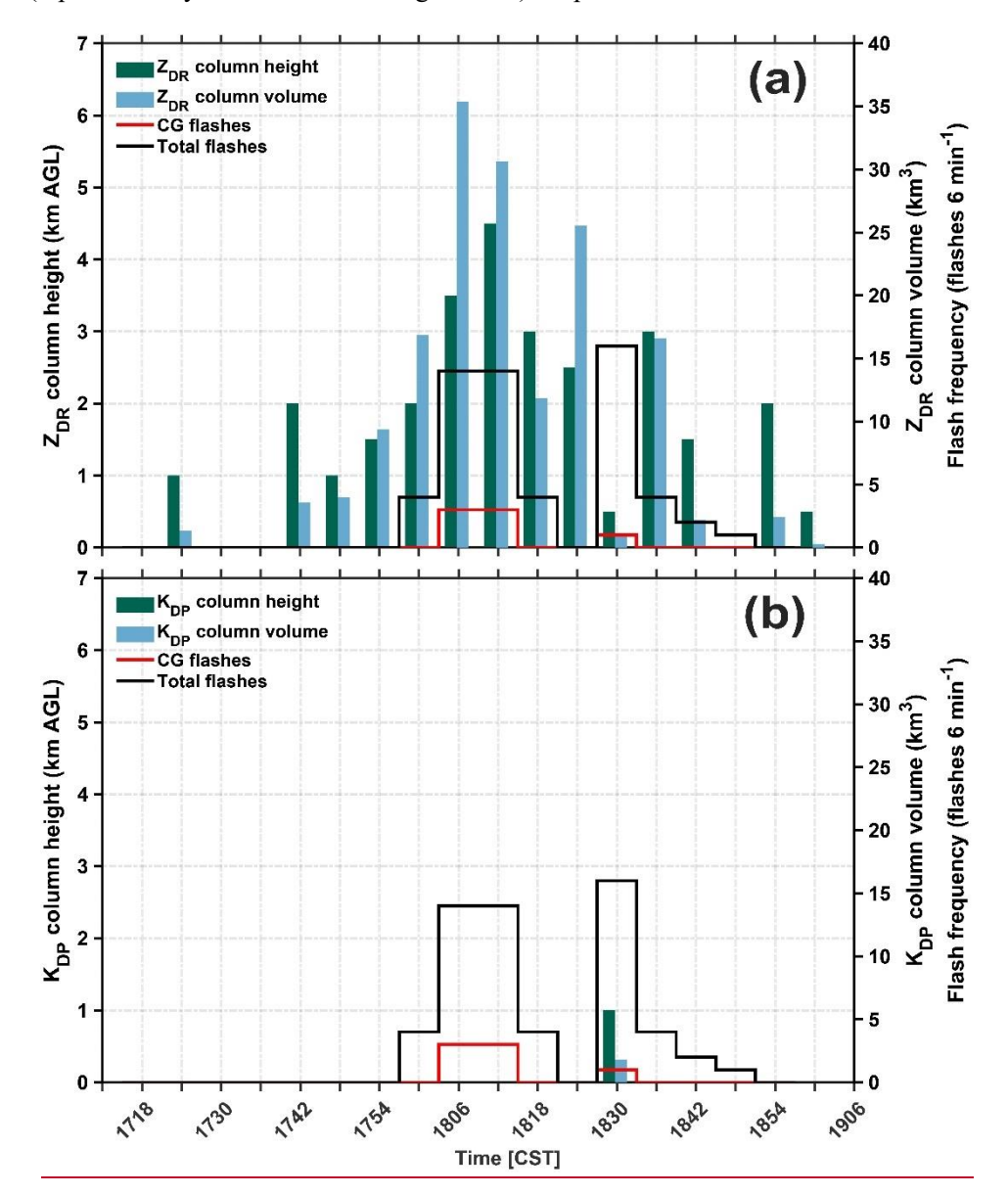


Figure 5. Time–height (volume) variation in the  $Z_{DR}$  column (a) and  $K_{DP}$  column (b). The dark green bars indicate the column heights and the light blue bars indicate the column volumes. The black (red) stepped line indicates the total flashes (CG flashes) from the LFEDA. AGL (above ground level).

Although large ice particles form and fall, the  $K_{DP}$  column is absent. However, a  $K_{DP}$  core with high values ( $\geq 1^{\circ}$ /km) occurs near the location where large ice particles (approximately 50 dBZ) melt, and a shedding process <u>may</u> occurs, resulting in a  $K_{DP}$  core (Figure 4e). At 18:30 CST, the

lightning activity reaches the second peak (Figure 65), but the Z<sub>DR</sub> column almost disappears; interestingly, the K<sub>DP</sub> column forms, with high values expanding downwards to the bottom of the cloud (Figure 4d, f). Thus, we suspect that K<sub>DP</sub> column in this study may have formed on the basis of the raindrops (1–2 mm) shed from hailstones melting in the warm phase region, which recirculated into the updrafts and were lifted to the mixed phase region. In addition, the K<sub>DP</sub> column only occurs at 18:30 CST, which corresponds to the second peak of lightning activity (Figure 5b).

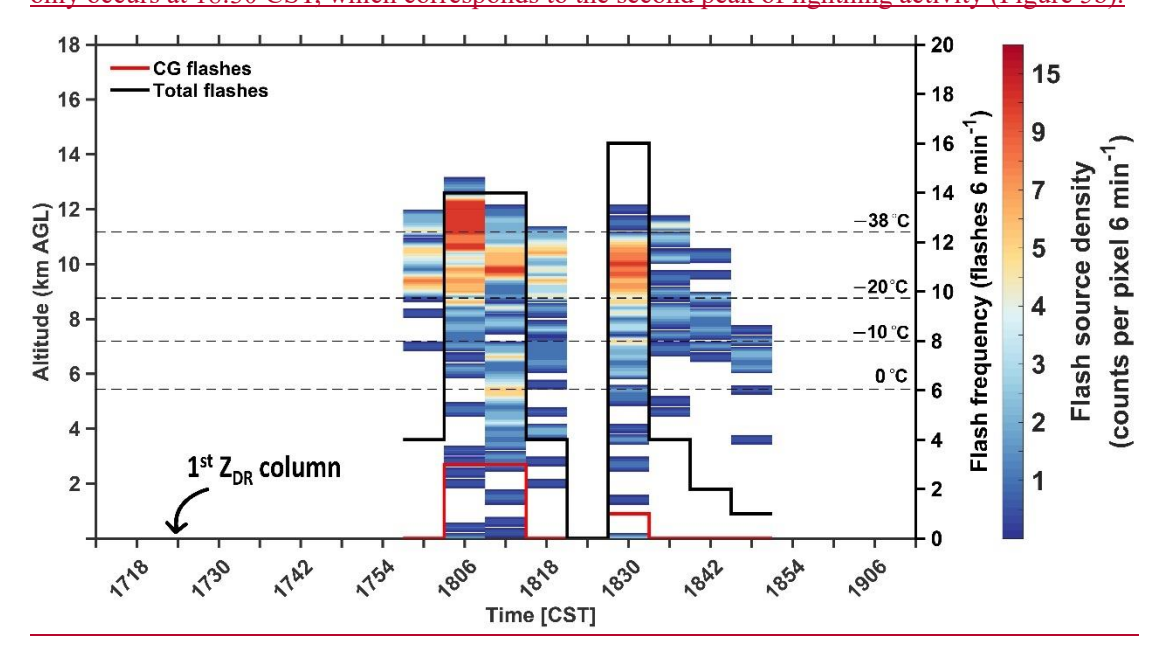


Figure 65. Time-height variation in flash source density (count per pixel, 6 min<sup>-1</sup>). The black (red) stepped line indicates the total flashes (CG flashes) from the LFEDA. The dashed lines indicate the isotherm heights from 0 to -38°C. AGL (above ground level).

#### 3.2 Vertical structures of microphysics related to lightning activity

To study the vertical thunderstorm structure related to lightning activity, we explore the vertical structures of polarimetric radar variables and microphysics, in combination with 3D lightning location data. Figure 7 displays the cross sections of polarimetric radar variables ( $Z_H$ ,  $Z_{DR}$ , and  $K_{DP}$ ) and microphysics (hydrometeor types and microphysical fingerprints) from the Cartesian grid of the studied isolated thunderstorm. At 18:00 CST (Figure 7 a1-e1), the lightning activity begins, and the locations of the flash sources are high and correspond mainly to graupel particles. Riming occurrence surrounds the flash sources. The  $Z_{DR}$  column and reflectivity core ( $\geq$  40 dBZ) begin to separate, having previously been overlapping during the initial development stage of the thunderstorm (Figure 4a, b). Then, at 18:06 CST (Figure 7 a2-e2), riming begins obviously, the

echoes strengthen ( $\geq$  55 dBZ), and the heights of the strong echoes are lifted. This finding indicates that the convective strength or updrafts are obviously increased and that the cold cloud processes are heavily. The lightning activity reached the first peak, where the locations of the flash sources mainly corresponded to graupel and ice particles. Moreover, the  $Z_{DR}$  column is located at the periphery of the reflectivity core, and high  $K_{DP}$  values occur and correspond to heavy rain particles, which are associated with large ice particles (e.g., hailstones) melting, raindrops coalescence and/or break. This phenomenon is consistent with that the  $K_{DP}$  tends to be directly proportional to the rain mixing ratio (Snyder et al., 2017).

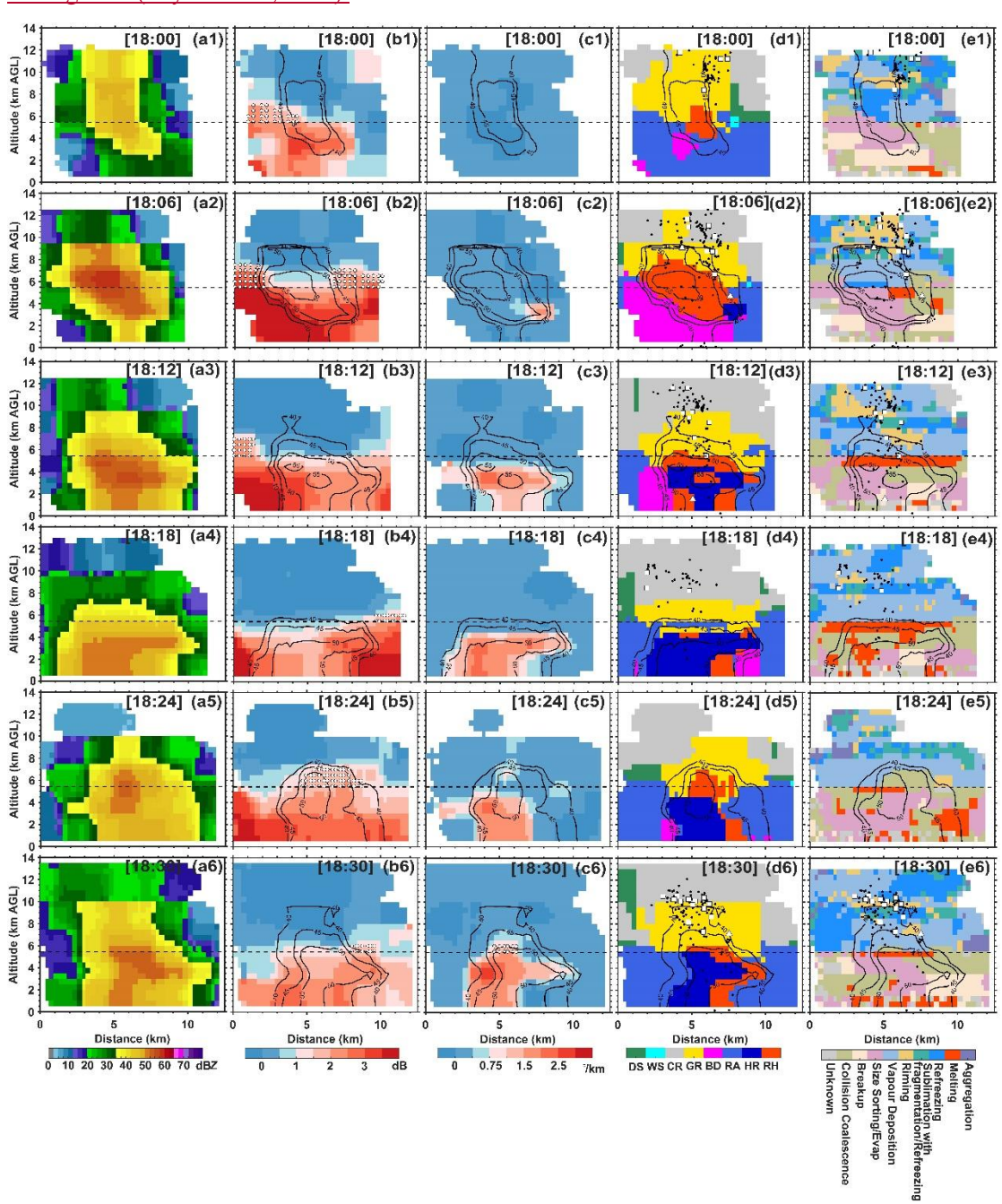


Figure 7. Cross sections of polarimetric radar variables (Z<sub>H</sub>, Z<sub>DR</sub>, and K<sub>DP</sub>) and microphysics (hydrometeor types and microphysical fingerprints) from the Cartesian grid of the isolated thunderstorm (case #1). At 18:00 CST (a1e1), 18:06 CST (a2-e2), 18:12 CST (a3-e3), 18:18 CST (a4-e4), 18:24 CST (a5-e5), and 18:30 CST (a6-e6). The black dashed line indicates the 0°C isotherm height. The white dots indicate the areas of the identified Z<sub>DR</sub>/K<sub>DP</sub>\_ columns. The black contours with values indicate the reflectivity structure. The black dots indicate the flash sources, the white square represents the first source of the intracloud flash, and the triangle represents the CG <u>flash.</u>

476

470

471

472

473

474

475

477

478

479

480

481

482

483

484

485

486

487

488

489

490

491

492

493

494

495

496

497

498

Subsequently, the lightning activity weakened at 18:12 and 18:18 CST. During this stage (Figure 7 a3-e3, a4-e4), the reflectivity core is landing and large ice particles above the melting level decrease, corresponding to heavy melting and indicating increasing downdrafts. Although Z<sub>DR</sub> columns are present, they can only indicate updrafts around the reflectivity core. However, the reflectivity core was lifted again at 18:24 CST (Figure 7 a5). The contents of rain and hail mixtures and graupel clearly increased (Figure 7 d5). This indicates that the convective strength or updrafts are increased. Notably, the Z<sub>DR</sub> column and reflectivity core overlap again, just as occurred during the initial development of the thunderstorm (Figure 4a, b; Figure 7 b5). Although a few high K<sub>DP</sub> values occurred above the melting level, a K<sub>DP</sub> column formed during the next 6 minutes (Figure 7 c5, c6). At 18:30 CST (Figure 7 a6-e6), the lightning activity reaches the second peak, and the riming process surrounds these flash sources. The Z<sub>DR</sub> column within the reflectivity core quickly collapses with the occurrence of abundant graupel particles.

In total, this thunderstorm shows two impulses in vertical velocity, which correspond to two lightning activity peaks. When the first impulse event initially develops, the Z<sub>DR</sub> column is obvious and overlaps with the reflectivity core; however, the region of the Z<sub>DR</sub> column within the reflectivity core will collapse, with abundant graupel particles forming by riming or freezing, stimulating updrafts and intensified lightning. When large ice particles (e.g., graupel or hailstone) subsequently decrease, indicating the end of the first impulse event, melting and shedding processes occur, resulting in more raindrops (many moderate-to-large and small raindrops) contributing to high Z<sub>DR</sub>/K<sub>DP</sub> values. These raindrops could recirculate into the updrafts and be lifted to the mixed-phase region, forming the Z<sub>DR</sub> column first, and raindrops could transfer to abundant graupel and even hailstones, releasing latent heat and thus invigorating updrafts again (indicating the second impulse

event). However, the  $Z_{DR}$  column within the reflectivity core will collapse with increasing amounts of graupel and/or hailstone particles, but the  $K_{DP}$  column will occur; this can be explained by the increased  $K_{DP}$  values at the column top being associated with an increasing number of small-to-moderate hailstones with significant water fraction (Snyder et al., 2017). The lightning activity also reaches a peak value.

Thus, the  $Z_{DR}$  column within the reflectivity core is likely an indicator of imminent convection invigoration via latent heat release and then the formation of abundant graupel particles promotes lightning activity via noninductive charging; the  $K_{DR}$  column is highly related to cold cloud processes, replacing  $Z_{DR}$  column to indicate updrafts within the reflectivity core when obvious graupels and hailstones occur.

## 3.32. The polarimetric and microphysical characteristics within the Z<sub>DR</sub> columns

Figure  $\S 6$  shows the normalized distributions of the polarimetric and microphysical characteristics within the series of  $Z_{DR}$  columns during the life cycle of the studied thunderstorm. The  $Z_H$  values within the  $Z_{DR}$  columns range from approximately 10 to 55 dBZ; specifically, weak reflectivity is present in the initial phase of the thundercloud (Figure  $\S 6$ a). This suggests the use of the  $Z_H$  threshold value (e.g., 25, 40, or 35–50 dBZ) to help select  $Z_{DR}$  columns results in the loss of information, especially for the initial phase of clouds. The increase in reflectivity intensity within the  $Z_{DR}$  columns can be used to predict lightning activity, and the peaks in both reflectivity intensity and lightning activity are consistent. A strong reflectivity intensity peak is associated with a high number of lightning flashes (Figure  $\S 6$ a).

The  $Z_{DR}$  values within the  $Z_{DR}$  columns range from approximately 1.5 to 4 dB, and the increasing trend of the  $Z_{DR}$  values is consistent with the first peak of lightning activity but has a low correlation with the second peak of lightning activity (Figure 86b). The pattern of  $D_0$  within the  $Z_{DR}$  columns is similar to that of the  $Z_{DR}$  values, depending on the strong linear relationship between  $D_0$  and  $Z_{DR}$  (Figure 86c). The liquid water content within the  $Z_{DR}$  columns ranges from approximately 0.1 to 4 gm<sup>-3</sup>, and the peaks correspond to the two peaks of lightning activity (Figure 86d). However, the relationship between the liquid water content within the  $Z_{DR}$  columns and the lightning flash frequency is not as strong as that between the  $Z_H$  values within the  $Z_{DR}$  columns and the lightning flash frequency.

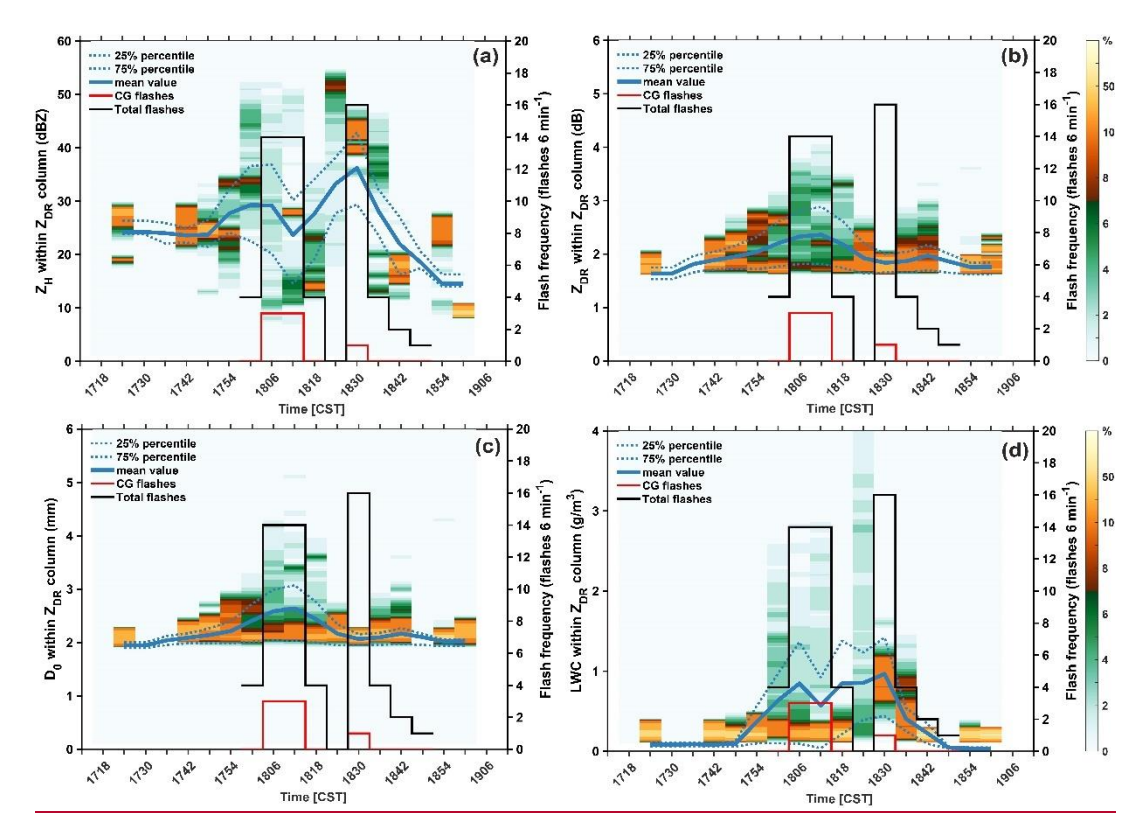


Figure <u>86</u>. The normalized distributions of the polarimetric and microphysical characteristics within the series of Z<sub>DR</sub> columns. (a) Z<sub>H</sub>. (b) Z<sub>DR</sub>. (c) <u>Median volume diameter (D<sub>0</sub>) of raindrops Liquid water content (LWC)</u>. (d)\_

<u>Liquid water content (LWC) Median volume diameter (D<sub>0</sub>) of raindrops</u>. The blue solid line indicates the mean value. <u>The shading indicates the normalized occurrence frequency (unit: %)</u>. The blue dashed lines indicate the 25% and 75% percentiles. The black (red) stepped line indicates the total flashes (CG flashes) from LFEDA, and the lightning flash frequency is counted every 6 minutes.

In addition, the percentage of hydrometeors within the  $Z_{DR}$  columns is investigated on the basis of the retrieved contents of ice (including graupel) or raindrops, as described in Section 2b. The results of hydrometeor identification are dominated by large size particles. Thus, we count the grids of ice (graupel) or raindrops via the results of the  $Z_{DP}$  method to investigate the percentage of hydrometeors within the  $Z_{DR}$  columns, avoiding neglecting the grid that possesses both ice (graupel) particles and liquid drops simultaneously. The obvious phenomenon is that the percentage of graupel within the  $Z_{DR}$  columns suddenly peaks before the first peak of lightning activity, but the second peak of lightning activity is not related to the presence of graupel within the  $Z_{DR}$  columns; the hydrometeor type within the  $Z_{DR}$  column at 18:30 CST is raindrops (Figure 97). Notably, the results neglect raindrops that smaller than 1 mm; although these small raindrops are a minor within the  $Z_{DR}$  column. This indicate the collapse of the  $Z_{DR}$  column within the reflectivity core at 18:30 CST,

which is consistent with the results shown in Figure 4d; the large-sized ice particles (i.e., graupel, corresponding to the reflectivity core) fall from aloft, and the smaller  $Z_{DR}$  values of such ice particles result in this collapse phenomenon. Thus, the retained  $Z_{DR}$  column corresponds to the periphery of the reflectivity core, indicating relatively weak updrafts and raindrops. Notably, the absence of graupel within the  $Z_{DR}$  columns does not mean that the graupel particles are eliminated within the clouds. On the other hand, the sudden increase in graupel within the  $Z_{DR}$  column at 18:00 CST may support the presence of a coalescence—freezing mechanism that led to graupel formation in the warm-based clouds. The hypothesis about coalescence—freezing mechanism was proposed in previous studies (e.g., Braham, 1986; Bringi, et al., 1997; Carey and Rutledge, 2000; Herzegh and Jameson, 1992).

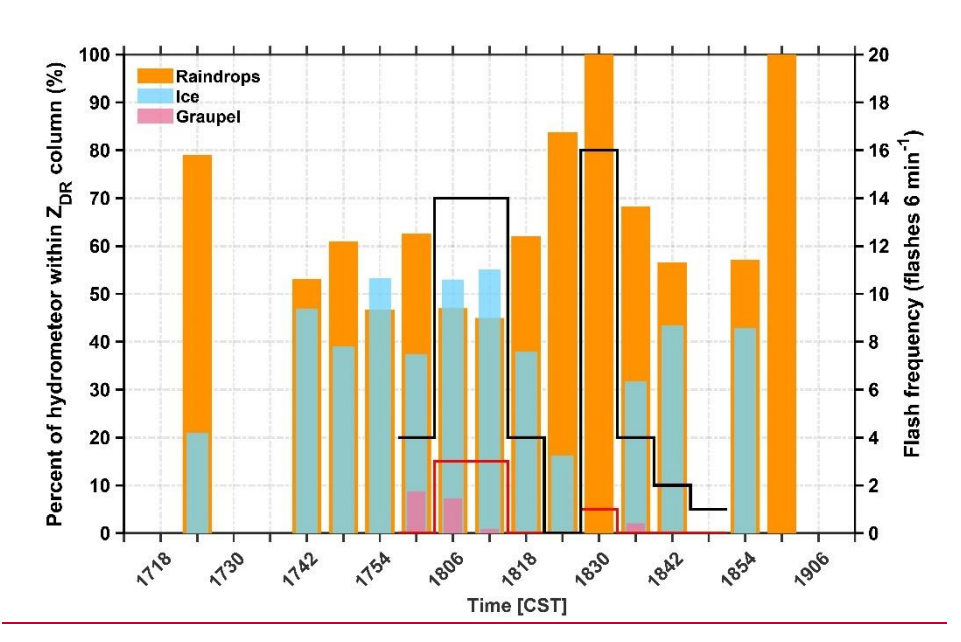


Figure 27. The percentages of hydrometeors within the series of Z<sub>DR</sub> columns. The orange bars indicate the percentage of raindrops. The blue bars indicate the percentage of ice particles (including graupel). The pink bars indicate the percentage of graupel. The black (red) stepped line indicates the total flashes (CG flashes) from LFEDA, and the lightning flash frequency is counted every 6 minutes.

## 3.3. Relationship between lightning activity and quantified ZDR columns

To determine the relationship between lightning activity and the quantified  $Z_{DR}$  columns, the height and volume of the  $Z_{DR}$  column are calculated via the "3D mapping column" method; the volume is based on the accumulation of all grids within the  $Z_{DR}$  column, and the volume of a single grid is 0.03125 km<sup>3</sup>, with 0.25 km horizontal and 500 m vertical resolutions. The height of the  $Z_{DR}$ 

column is determined by counting the grid number (n) from the freezing level to the highest grid within the  $Z_{DR}$  column; if n is determined, the  $Z_{DR}$  column height is  $n \times 0.5$  km. Figure 108a displays the variations in the lightning flash frequency and  $Z_{DR}$  column height. Thevariation trend of the lightning activity before the second peak is highly consistent with the trend-of the  $Z_{DR}$  column height. However, these trends seem to be in sync, which is not beneficial forforecasting lightning activity. The cross-correlation approach can be used to examine the correlation considering the time lag, which is important for verifying whether a parameter is appropriate for forecasting another parameter. Figure 108b shows the cross-correlation between lightning activity and the  $Z_{DR}$ -column height. The highest correlation coefficient ( $-\le 0.8$ ) between lightning activity and the  $Z_{DR}$ -column height is observed at a lag time of -6 minutes; thus, the variation in lightning activity occurs before that in the  $Z_{DR}$ -column height (Figure 108b). However, it should be emphasized that the trend toward confidence is more important than the timing of the maximum correlation.

## 3.4. Statistical results

To determine the relationship between lightning activity and the quantified  $Z_{DR}$  columns, the height and volume of the  $Z_{DR}$  column are calculated via the "3D mapping column" method; the volume is based on the accumulation of all grids within the  $Z_{DR}$  column, and the volume of a single grid is 0.03125 km³, with 0.25-km horizontal and 500-m vertical resolutions. The height of the  $Z_{DR}$  column is determined by counting the grid number (n) from the melting level to the highest grid within the  $Z_{DR}$  column; if n is determined, the  $Z_{DR}$  column height is  $n \times 0.5$  km.

The variations in the Z<sub>DR</sub>/K<sub>DP</sub> column height and volume with the life cycle of the remaining fourteen cases are displayed in Figures 10 (cases #2 to #8) and 11 (cases #9 to #15), as are the variations in the percentages of hydrometeor types and microphysical fingerprints. The grid is assigned to specific particle type based on the results of hydrometeor identification, and the percentage of grids for each hydrometeor type is calculated. Similarly, this process is applied to determine the percentage of grids associated with microphysical fingerprints. Each of them has a Z<sub>DR</sub> column (Figure 10 a1-a7, Figure 11 a1-a7); however, the absence of a K<sub>DP</sub> column is possible (Figures 10 b1-b7, Figures 11 b1-b7). The results of our study support the observations of Bruning et al. (2024), namely, lightning is not observed in the absence of a Z<sub>DR</sub> column, and a K<sub>DP</sub> column

is not observed without a  $Z_{DR}$  column. Moreover, the highest lightning flash frequency (in case #11) is observed when the  $Z_{DR}$  and  $K_{DP}$  columns are co-present, which is consistent with the observations of Bruning et al. (2024). In addition, our results suggest that the signal in the  $K_{DP}$  column within these small, isolated, subtropical thunderstorms over South China is not as steady as that in the  $Z_{DR}$  column during the life cycle.

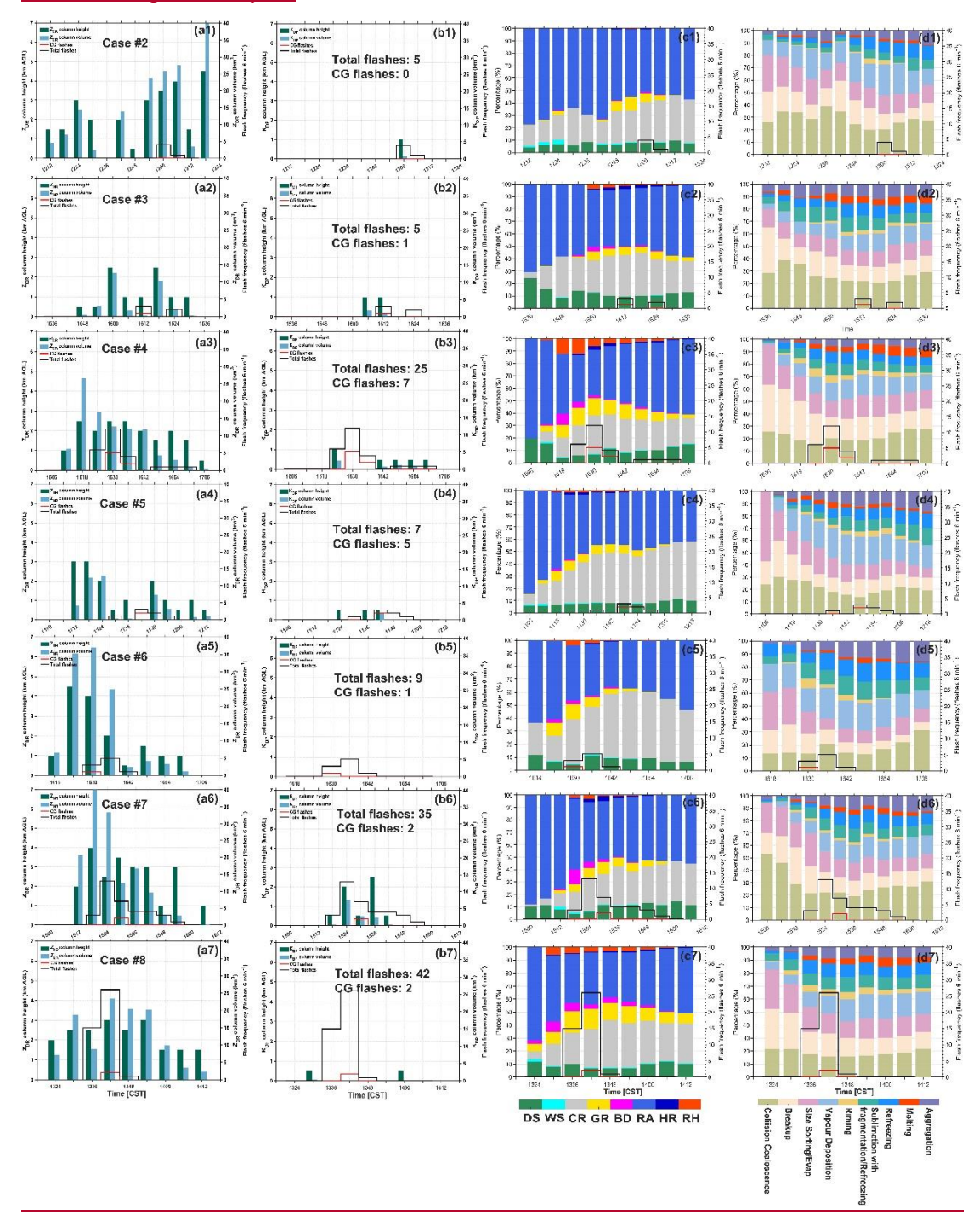


Figure 10. The variation in  $Z_{DR}$  column height and volume with the life cycle of thunderstorms (cases #2 to #8) (a1-a7). The variation in the  $K_{DP}$  column height and volume with the life cycle of thunderstorms (cases #2 to #8)

603	(b1-b7). The dark green bars indicate the column heights, and the light blue bars indicate the column volumes. The
604	texts display the number of total flashes and CG flashes in a thunderstorm. The variation in percentages of
605	hydrometeor types with the life cycle of thunderstorms (cases #2 to #8) (c1-c7). The variation in percentages of
606	microphysical fingerprints with the life cycle of thunderstorms (cases #2 to #8) (d1-d7). The black stair lines
607	indicate the total flashes, and the red stair lines indicate the CG flashes.
608	The results show that the percentages of identified graupel particles and riming process are
609	closely related to lightning activities (Figures 10 c1-c7, d1-d7 and Figures 11 c1-c7, d1-d7), which
610	are consistent with that in Figure 7. The cross-correlation approach can be used to examine the
611	correlation considering the time lag, which is important for verifying whether a parameter is
612	appropriate for forecasting another parameter. To further determine the correlation between
613	lightning activity and the polarimetric structure. The cross correlations between the lightning
614	activity and polarimetric structure during the life cycles in all the cases are examined, and the results
615	are displayed in Figure 12.

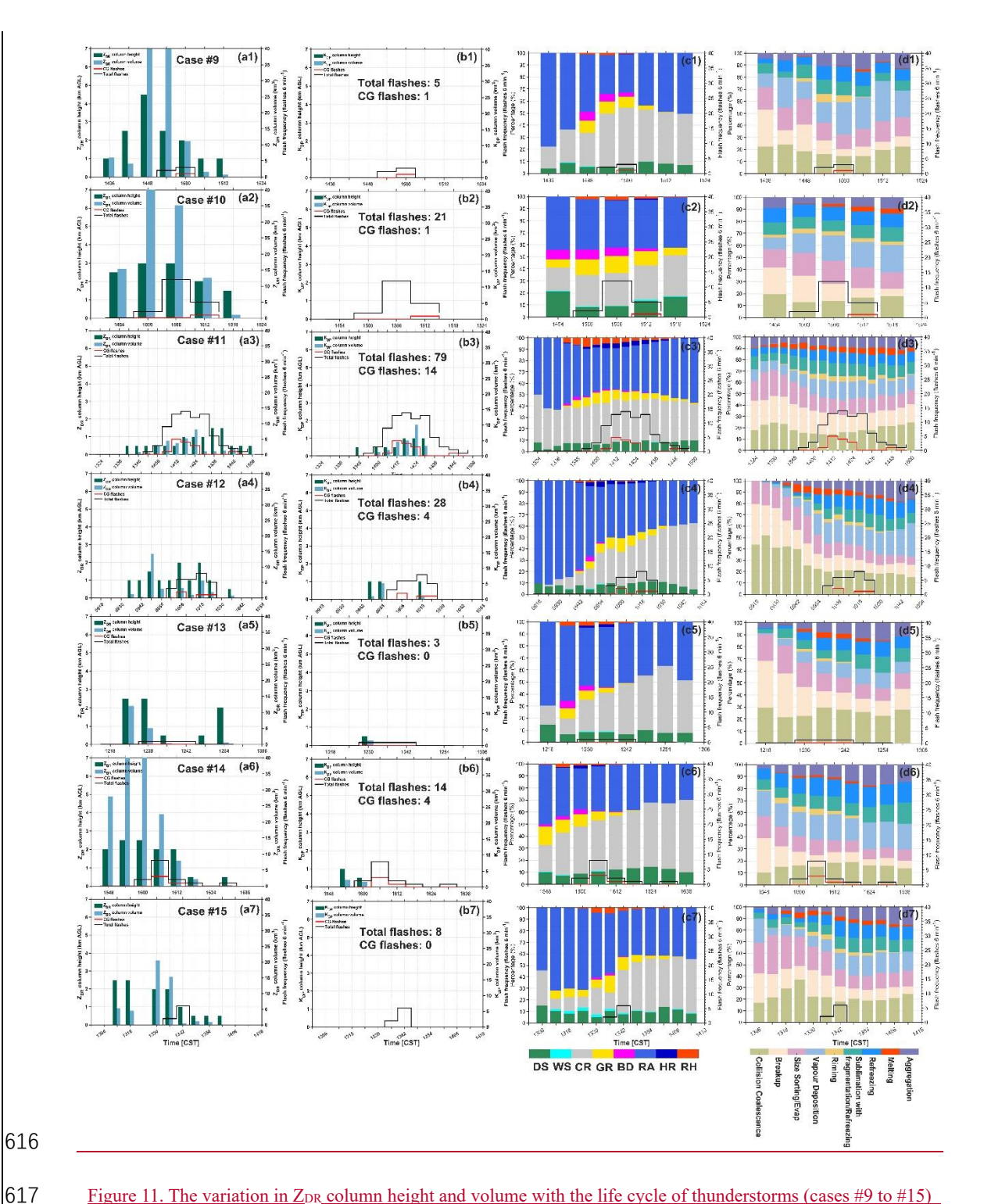


Figure 11. The variation in Z<sub>DR</sub> column height and volume with the life cycle of thunderstorms (cases #9 to #15)

(a1-a7). The variation in the K<sub>DP</sub> column height and volume with the life cycle of thunderstorms (cases #9 to #15)

(b1-b7). The dark green bars indicate the column heights, and the light blue bars indicate the column volumes. The texts display the number of total flashes and CG flashes in a thunderstorm. The variation in percentages of hydrometeor types with the life cycle of thunderstorms (cases #9 to #15) (c1-c7). The variation in percentages of

622	microphysical fingerprints with the life cycle of thunderstorms (cases #9 to #15) (d1-d7). The black stair lines
623	indicate the total flashes, and the red stair lines indicate the CG flashes.
624	Figure 12a shows that the variation in the graupel or rain water content above the melting level
625	within the cloud can predict the lightning activity (total flashes) after 6 minutes well, and the
626	correlation coefficient is approximately 0.8. However, other parameters (e.g., Z <sub>DR</sub> column volume)
627	ice content above the melting level, and graupel volume) also exhibit good performance in
628	forecasting lightning activity, and the correlation coefficient can reach approximately 0.7. The
629	graupel volume is calculated based on the identification results of hydrometeors. Although the
630	variation in the graupel or rain water content above the melting level within the cloud can also
631	forecast the lightning activity (CG flashes) after 6 minutes, the correlation coefficient decreases to
632	approximately 0.56 (Figure 12b). Notably, the trend of the Z <sub>DR</sub> column volume implies that it may
633	perform well with a longer warning time (e.g., 12 minutes) for lightning activity.

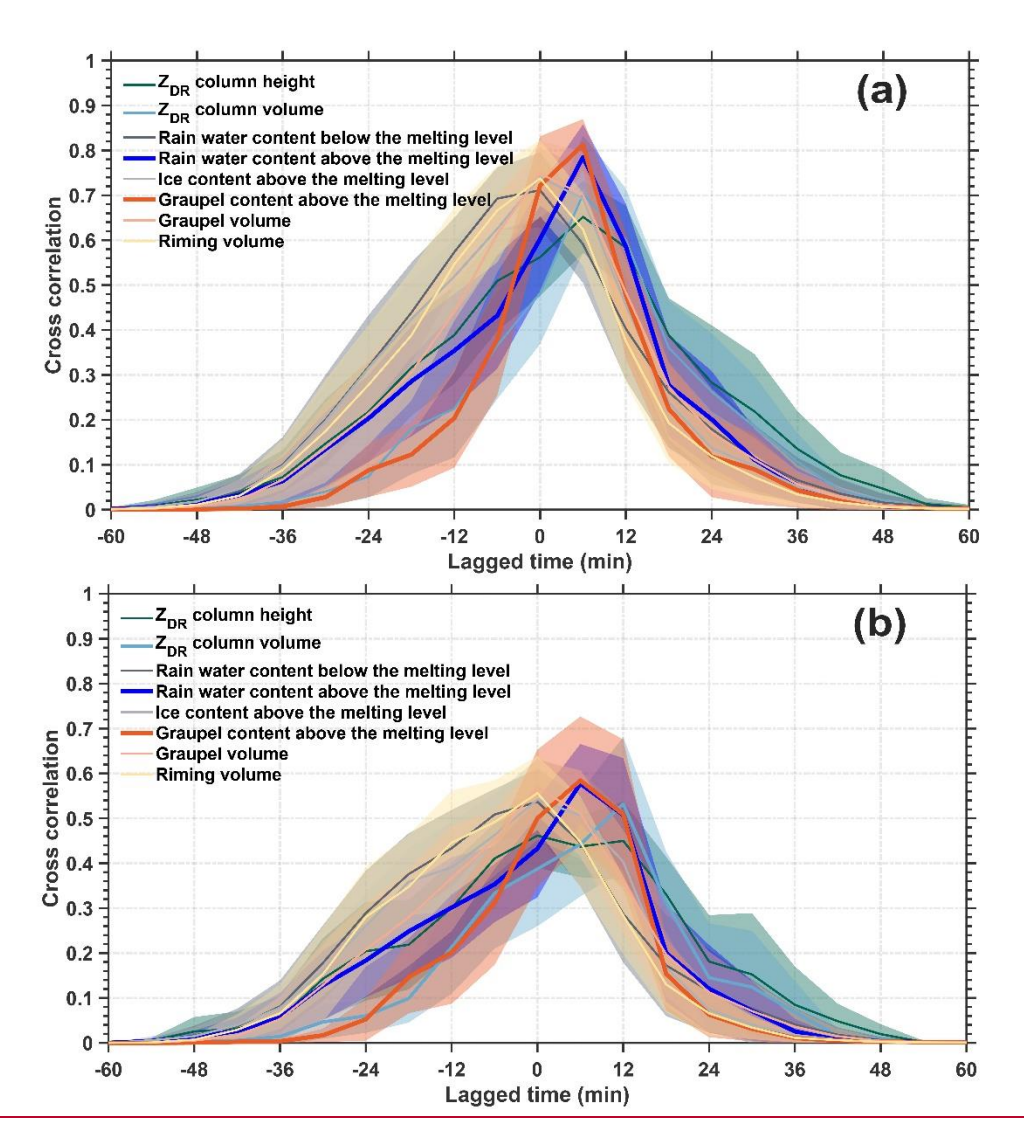


Figure 12. Cross-correlations between flash frequency (total flashes (a), CG flashes (b)) and eight radar-retrieved variables (Z<sub>DR</sub> column height/volume, rain water content below/above the melting level, ice content above the melting level, graupel volume, and riming volume); the lines indicate the mean values and the shaded area indicates the 95% confidence interval. The lagged time is for flash frequency lags these eight radar-retrieved variables.

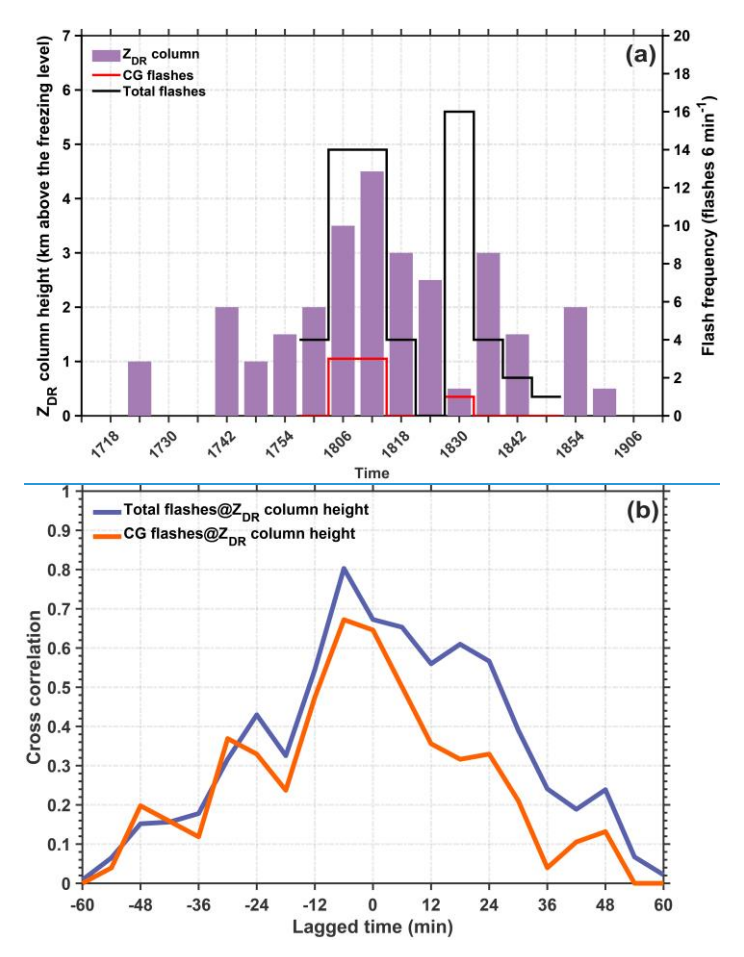


Figure 8. (a) The variation in the Z<sub>DR</sub>-column height with time. The purple bars indicate the heights of the Z<sub>DR</sub>-columns. The black (red) stepped line indicates the total flashes (CG flashes) from LFEDA, and the lightning flash frequency is counted every 6 minutes. (b) Cross correlation between flash frequency and Z<sub>DR</sub>-column height; the blue and orange lines indicate the total flashes and CG flashes, respectively.

Figure 9 shows the relationship between lightning activity and the Z<sub>DR</sub>-column volume, and the variation trend in the second peak of lightning activity is indistinguishable via the variation trend in the Z<sub>DR</sub>-column volume (Figure 9a); this finding is similar to that shown in Figure 8a. The highest correlation coefficient between the lightning activity and Z<sub>DR</sub>-column volume is improved (~0.84 for the total flashes and 0.75 for CG flashes); specifically, the variation trend of the Z<sub>DR</sub>-column height can be used to predict the lightning activity (total flashes) after 6 minutes (Figure 9b).

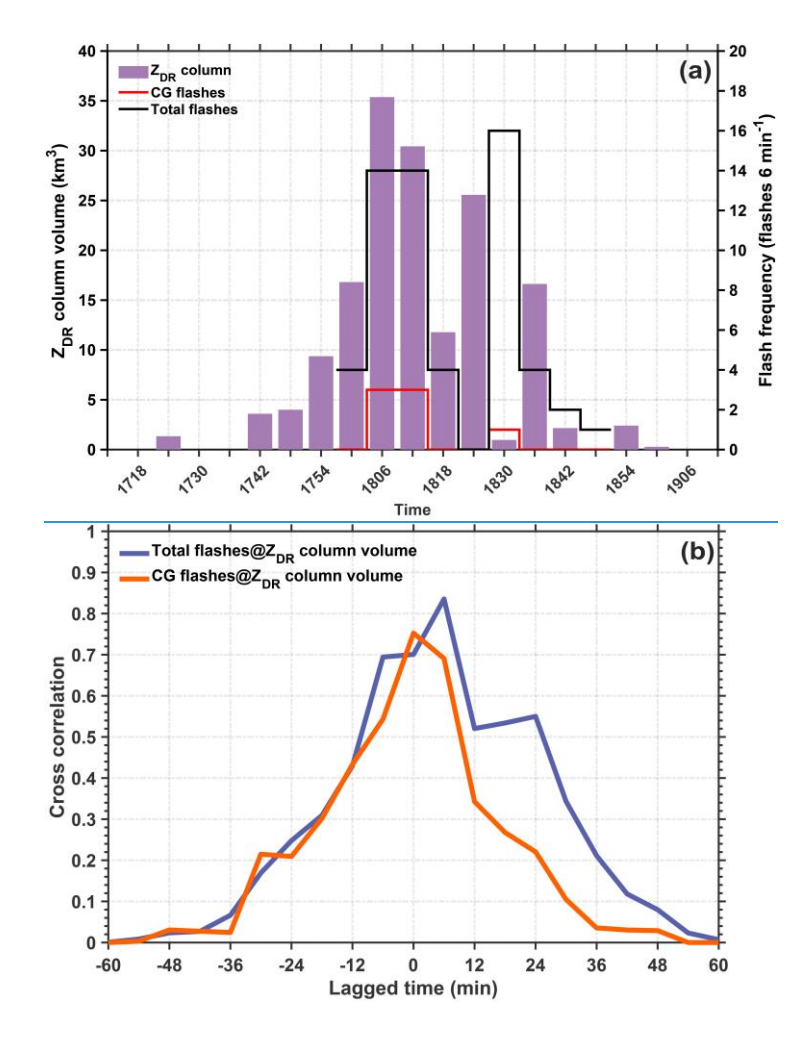


Figure 9. The same as in Figure 8 but for the ZDR column volume.

## 3.4. Relationship between lightning activity and ice (liquid) microphysics

The microphysical characteristics of ice or liquid should exhibit a strong relationship with lightning activity on the basis of a noninductive charging mechanism. As expected, Figure 120 indicates that the variation in the rain water content above the freezing level within the cloud can be better used to forecast lightning activity (total flashes) than can the variation in the Z<sub>DR</sub> column volume. The highest correlation coefficient between the lightning activity (total flashes) and supercooled liquid water reaches approximately 0.93, and the lightning activity lag time is 6 minutes. Figure 11 shows that the variation in the ice or graupel content above the freezing level within the cloud can indicate the lightning activity (total flashes) in real time, and the highest correlation coefficient between the lightning activity (total flashes) and the ice content is 0.84–0.89. However, the graupel content above the freezing level within the cloud is the best indicator for forecasting lightning activity (CG flashes); the highest correlation coefficient between lightning activity (CG

flashes) and the graupel content is approximately 0.86, and the trend of CG flashes lags behind the variation in graupel content above the freezing level within the cloud, with a lag time of 6 minutes.

Therefore, the content of supercooled liquid water within the cloud is the best proxy for

forecasting lightning activity (total flashes) after 6 minutes; the graupel content above the freezing level within the cloud is the best proxy for forecasting the lightning activity (CG flashes) after 6 minutes.

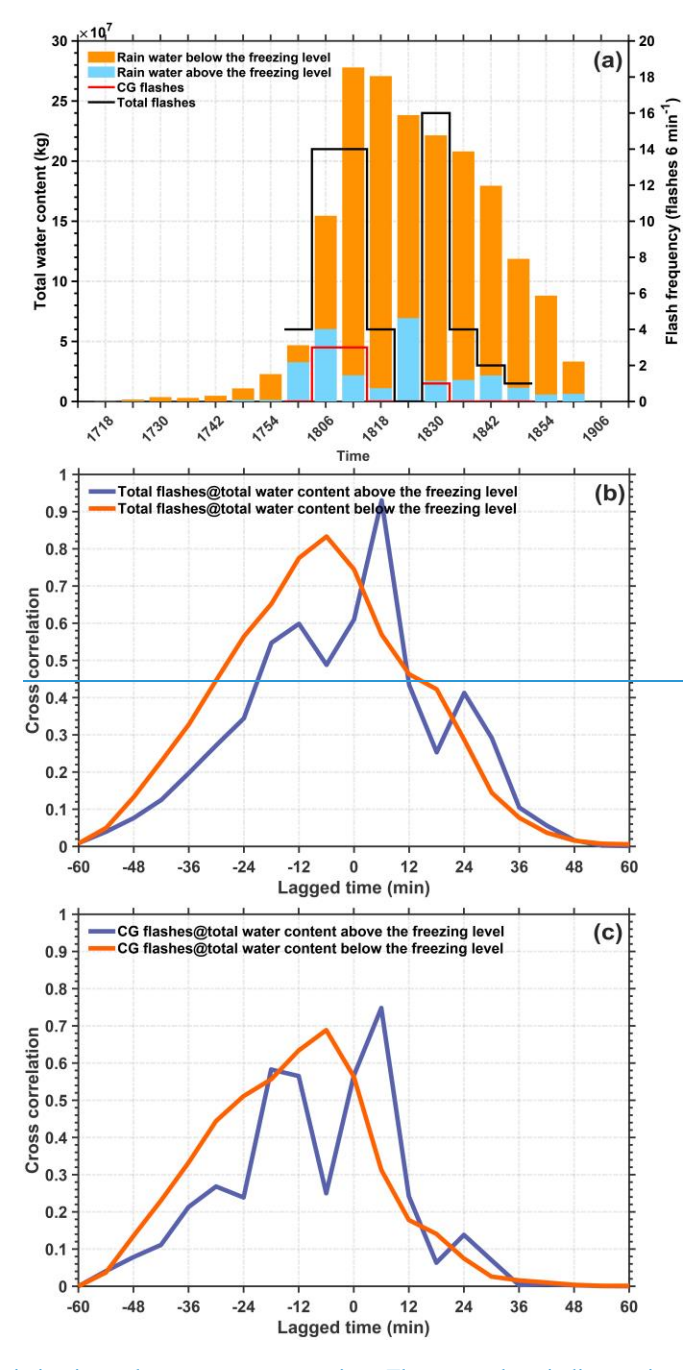


Figure 10. (a) The variation in total water content over time. The orange bars indicate rainwater below the freezing level. The blue bars indicate rainwater above the freezing level. (b) Cross-correlation between flash frequency and

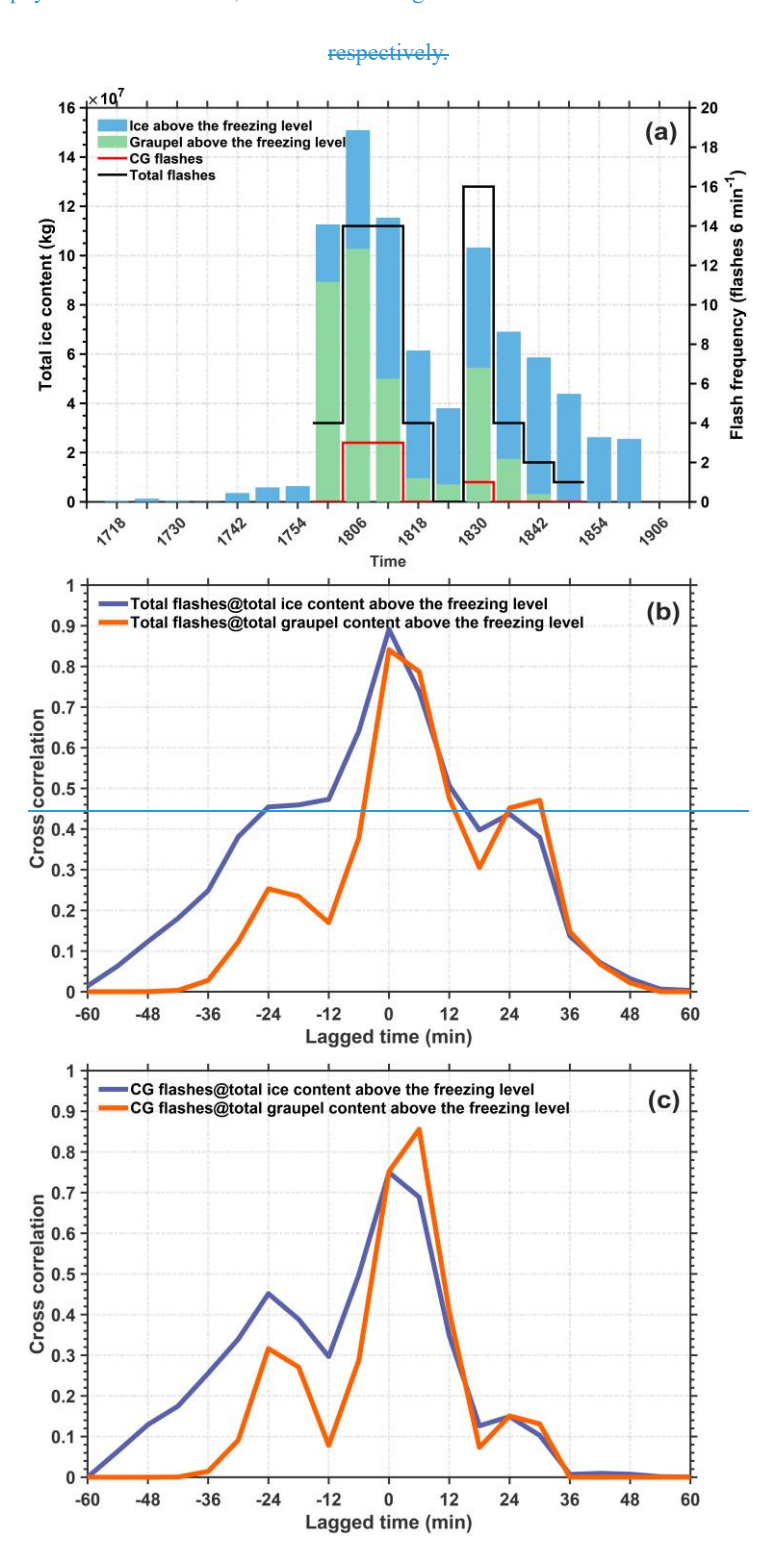


Figure 11. The same as in Figure 10 but for the total ice content.

#### 4. Conclusion and discussion

The relationship between the polarimetric structure and lightning activity is

evaluated investigated within fifteenan isolated thunderstorm cells during the cloud life cycle in this study. We focus on the proxies of cloud updrafts and supercooled liquid raindrops ( $Z_{DR}$  or  $K_{DP}$  columns) and the content of ice or rainwater, which have been demonstrated to be related to the variations in the number of lightning flashes in previous studies (e.g., Bruning et al., 2024; Carey and Rutledge, 2000; Hayashi et al., 2021; Sharma et al., 2024; Sharma, et al., 2021; van Lier-Walqui, et al., 2016). Furthermore, we explore the microphysical fingerprints, which should be related to column formation and lightning activity. Therefore, the objective of this study is to clarify the sequence and interactions of these parameters for predicting lightning activity during the cloud life cycle and understanding the corresponding cloud microphysics.

681

682

683

684

685

686

687

688

689

690

691

692

693

694

695

696

697

698

699

700

701

702

703

704

705

706

707

708

To precisely identify and quantify the Z<sub>DR</sub> or K<sub>DP</sub> columns within an isolated thunderstorm during the whole cloud life cycle, the "3D mapping columns" method is improvedestablished; it is based on the morphology and high values of the ZDR or KDP columns in Cartesian grid data. The "3D mapping columns" method has advantages in identifying Z<sub>DR</sub> columns in the initiation phase of convective clouds, avoiding the utilization inappropriate threshold value of Z<sub>H</sub>. The volume and height of the Z<sub>DR</sub> columns are quantified via the "3D mapping columns" method, and the correlation coefficient indicates that the volume of the  $Z_{DR}$  column is better for forecasting lightning activity than the column height is. In addition, both the volume and height of a Z<sub>DR</sub> column have some limitations in forecasting lightning activity, except during the early phase. This phenomenon is similar to the results of Sharma et al. (2024). In their study, the correlation coefficient between the Z<sub>DR</sub> column volume and total flash rate generally monotonically decreased after the initial lightning jump, and the volume of the K<sub>DP</sub> columns exhibited relatively high co-variability with the total flash rate, except in the early phase. The time lag between the formation of the Z<sub>DR</sub> column and that of the K<sub>DP</sub> column was consistent with the results of this study, indicating the different formation mechanisms of the Z<sub>DR</sub> and K<sub>DP</sub> columns described in Section 1. The moment of occurrence of the first Z<sub>DR</sub>-column can be determined at least 36 minutes prior to the first lightning flash (Figure 5), which is a substantial lead time for forecasting the first lightning flash; notably, the numerical value was usually 4-6 minutes in previous studies (e.g., Gremillion and Orville, 1999; Vincent et al., 2003; Mosier, et al., 2011).

The volume and height of Z<sub>DR</sub>-columns are quantified via the "3D mapping columns" method, and the correlation coefficient indicates that the volume of the Z<sub>DR</sub> column is better for forecasting lightning activity than is the column height. In addition, both the volume and height of a Z<sub>DR</sub> column have some limitations in forecasting lightning activity, except during the early phase. This phenomenon is similar to the results of Sharma et al. (2024). In their study, the correlation coefficient between the Z<sub>DR</sub> column volume and total flash rate generally monotonically decreased after initial lightning jump, and the volume of the K<sub>DP</sub> columns exhibited relatively high co-variability with the total flash rate, except in the early phase. The time lag between reported between the formation of the Z<sub>DR</sub> column and that of the K<sub>DP</sub> column was consistent with the results of this study, indicating the different formation mechanisms of the Z<sub>DR</sub> and K<sub>DP</sub> columns described in Section 1.

As discussed in Section 3.2, lightning activity is indeed related to dynamic variation and impulses in vertical velocity, which is consistent with the findings of previous studies (e.g., Bruning et al., 2024; Sharma et al., 2021). The unsteady Z<sub>DR</sub> and K<sub>DP</sub> columns are tied to unsteady updrafts associated with thermal bubbles, which are relatively short-lived and thus

impulses in vertical velocity, which is consistent with the findings of previous studies (e.g., Bruning et al., 2024; Sharma et al., 2024; Sharma et al., 2021). The unsteady  $Z_{DR}$  and  $K_{DP}$  columns are tied to unsteady updrafts associated with thermal bubbles, which are relatively short-lived and thus indicate an impulse in vertical velocity. In this way, the variations in the  $Z_{DR}$  and  $K_{DP}$  columns can indicate lightning activity. Although this hypothesis is reasonable and supported by observations through the microphysical signatures of large-drop lofting and glaciation corresponding to the  $Z_{DR}$  and  $K_{DP}$  columns (Bruning et al., 2024; Fridlind et al., 2019); however, the observations of Sharma et al. (2024) and Sharma et al. (2021) revealed that the  $K_{DP}$  column volumes (or mean  $K_{DP}$  values within a segmented  $K_{DP}$  column) have noticeably different pattern than the  $Z_{DR}$  column volumes (or mean  $Z_{DR}$  values within a segmented  $Z_{DR}$  column), which has remained a question in Sharma et al. (2021).

In this study, we explore the polarimetric and microphysical structures related to impulse events and lightning activity. The results indicate that the column within the reflectivity core is only the  $Z_{DR}$  column in which the impulse event initially develops; then, the supercooled raindrops indicated by the  $Z_{DR}$  column transfer to abundant graupel and/or hailstone particles, releasing latent heat and thus invigorating convection; accompanying the  $Z_{DR}$  column within the reflectivity core, it collapses, and lightning intensifies. Moreover, the formation of the  $K_{DP}$  column requires melting and shedding processes from large ice particles (e.g., graupel or hailstones) that produce many

raindrops of moderate-to-large and small sizes, which contribute to high  $Z_{DR}/K_{DP}$  values. These raindrops can recirculate into updrafts and be lifted to the mixed-phase region, forming the  $Z_{DR}$  column first, but then, it collapses as graupel and/or hailstone particles increase. Convection and lightning are enhanced, and a  $K_{DP}$  column is formed, which is associated with an increasing number of small-to-moderate hailstones with a significant water fraction. Thus, the  $Z_{DR}$  and  $K_{DP}$  columns within the reflectivity core are associated with the different stages of an impulse event, the  $Z_{DR}$  column indicates the stage in which cold cloud processes are weak, and the  $K_{DP}$  column is the opposite of the  $Z_{DR}$  column. This may explain the remaining question in Sharma et al. (2021), namely, why the  $K_{DP}$  column has a noticeably different pattern than the  $Z_{DR}$  column does. Notably, the  $Z_{DR}$  column is located at the periphery of the reflectivity core when the  $Z_{DR}$  column collapses within the reflectivity core.

As shown in Figure 4 and discussed in Section 3.1, we hypothesize that the K<sub>DP</sub> column may form on the basis of the raindrops (1–2 mm) that shed from hailstones melting in the warm phase region of clouds, which then recirculate into the updrafts and are lifted to the mixed phase region. This is different from the hypothesis proposed in previous studies (e.g., (Bringi, et al., 1996, Hubbert, et al., 1998, Loney, et al., 2002)). Thus, the presence of many or large hailstones in supercells may result in robust K<sub>DP</sub> columns (e.g., (Sharma, et al., 2024)); in contrast, short lifetimes and weak dynamics within isolated thunderstorm cells in this study result in single-moment K<sub>DP</sub> column.

Notably, our results indicate that the content of supercooled liquid water is the best variable for forecasting lightning activity (total flashes); the correlation coefficient is approximately 0.94, and the lead time is 6 minutes. For CG flash forecasting, the content of graupel displays the highest correlation coefficient (~0.86) with lightning activity, and the lead time is also 6 minutes. Similar results were reported by Carey and Rutledge (2000), suggesting that graupel particles are likely related to CG flash occurrence.

We bridged the polarimetric structure (the Z<sub>DR</sub>/K<sub>DP</sub> column, supercooled liquid water, and graupel content below 0°C) and lightning activity on the basis of observations of fifteen isolated thunderstorm cells (the variation curve is conceptualized in Figure 13). The two peaks of lightning activity in Figure 13 suggest multiple impulse events in convection; specifically, the first peak refers specifically to the initial impulse event, but the second peak suggests subsequent impulse events.

The magnitude of the amplitudes among these curves has no practical meaning; it is merely for visualization purposes.

# Heavily cold cloud processes

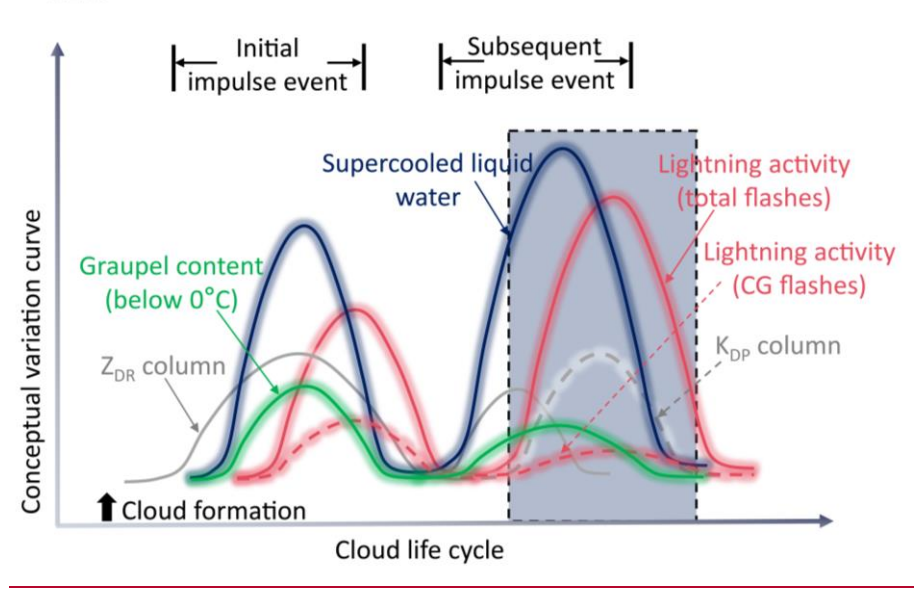


Figure 13. A conceptual model bridging the polarimetric structure and lightning activity.

In our opinion (Figure 13), the Z<sub>DR</sub> column within the reflectivity core is likely an indicator of imminent convection invigoration via latent heat release, after which the formation of abundant graupel particles promotes lightning activity via noninductive charging. Therefore, microphysics (e.g., graupel content) are more directly related to lightning activity than are dynamics (e.g., the Z<sub>DR</sub> column). Moreover, the observations reveal that the microphysical variations in supercooled liquid water and graupel yield better correlation coefficients for the prediction of lightning activity at short warning times (e.g., 6 minutes in this study) than do the dynamical variations in the Z<sub>DR</sub> column volume. However, the trend of the Z<sub>DR</sub> column volume implies that it may perform well with a longer warning time (e.g., 12 minutes in this study) for lightning activity. The K<sub>DR</sub> column is highly related to cold cloud processes. Thus, the K<sub>DP</sub> column is likely absent when the impulse event initially develops; however, it will be present later with heavily cold cloud processes, replacing the Z<sub>DR</sub> column to indicate updrafts within the reflectivity core when obvious graupels and hailstones are occurring. In addition, the 6-min or 12-min warning time in our results is likely due to the temporal resolution (6 minutes) of the radar data used in this study; high temporal resolution observations of phased-array radar may decrease the uncertainty.

Notably, the threshold value for identifying the  $Z_{DR}$  column ( $\geq 1.5$  dB) in this study is different from that ( $\geq 1$  dB) in previous studies (e.g., Sharma et al., 2024). Although this threshold value is selected according to the retrieved raindrop diameter, which should exceed 2 mm within the  $Z_{DR}$  column during the initial phase of a storm (Kumjian, et al., 2014), the results for quantifying the  $Z_{DR}$  column (i.e., height and volume) may be different from those of previous studies that used the 1 dB threshold (e.g., Sharma et al., 2024). However, this study focuses on the trend of the  $Z_{DR}$  column height or volume; thus, the differences resulting from different thresholds are relieved. The threshold value for identifying the  $K_{DP}$  column ( $\geq 1^{\circ}$ /km) in this study is consistent with that used by Sharma et al. (2024). However, the different estimation methods for  $K_{DP}$  may introduce additional uncertainty, as discussed in Sharma et al. (2021).

Moreover, the height of the melting layer (0°C), which is derived from environmental soundings, is assumed to be constant for identifying and quantifying the Z<sub>DR</sub>/K<sub>DP</sub> column; however, the melting level is frequently elevated within updraft cores because of latent heat release, which is influenced by the strength of updrafts relative to the ambient environment. Thus, a more accurate melting level will decrease the biased estimations of the "3D mapping columns" method in this study. In addition, although our results support some observations in Bruning et al. (2024) and seem to explain the remaining question in Sharma et al. (2024) and Sharma et al. (2021), whether there are differences between such small, isolated, subtropical thunderstorms and other thunderstorm types (i.e., mesoscale convective systems, supercells, or tropical thunderstorms) should be further analysed to reduce the probability of uncertainty in our study. Finally, although the results retrieved from hydrometeor identification and microphysical fingerprint methods are reasonable and obey theoretical cognition in this study, the potentially biased estimates may result from isothermal height and the status of the hydrometeor (e.g., canting angle).

the prediction of lightning activity should involve the content of supercooled liquid water and graupel. Specifically, the first occurrence of the Z<sub>DR</sub>-column can be used to forecast lightning initiation as early as possible. Owing to the time lag between the formation of the Z<sub>DR</sub> and K<sub>DP</sub> columns, the signatures of the Z<sub>DR</sub> and K<sub>DP</sub> columns should be coupled to retrieve dynamic information instead of lightning activity; specifically, the Z<sub>DR</sub> column is only suitable for the early phase of cloud development. We bridged the polarimetric structure (four important parameters

provided in previous studies) and lightning activity on the basis of observations of a thermodynamically dominated isolated thunderstorm cell (the variation curve is conceptualized in Figure 12).

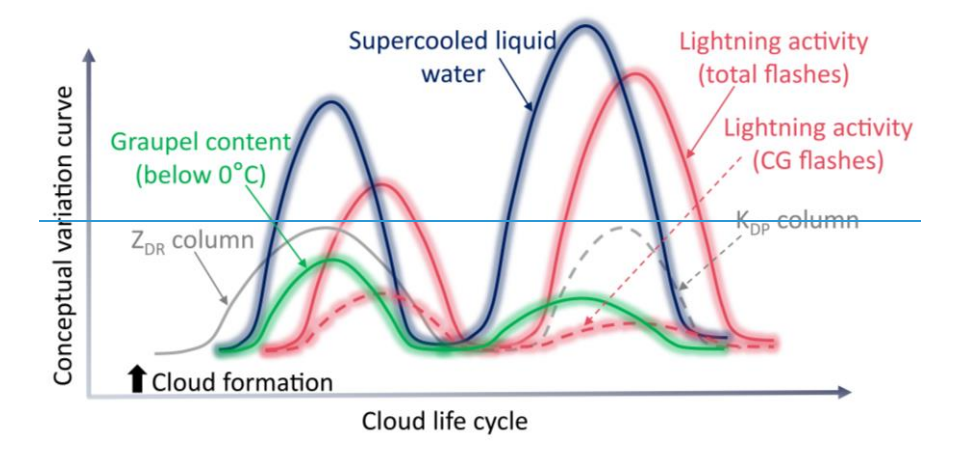


Figure 132. A conceptual model bridging the polarimetric structure and lightning activity.

Notably, the variation in the Z<sub>H</sub> intensity and liquid water content within the Z<sub>DR</sub> columns can be used to predict lightning activity during the cloud life cycle, and the former is a better preditor. However, this result is novel and has not been reported previously; therefore, substantial investigations should be performed to verify this finding in the future. Although this study is based on the results of previous studies (e.g., Carey and Rutledge, 2000; Krause and Klaus, 2024; Sharma et al., 2021; Snyder, et al., 2015; van Lier-Walqui, et al., 2016; Woodard et al., 2012), more types of thunderstorms and more samples should be analysed to reduce the probability of uncertainty in our study.

# Acknowledgments

We thank Prof. Bruning and the anonymous reviewer for their professional and constructive comments and suggestions. The authors—We acknowledge the Guangzhou Institute of Tropical and Marine Meteorology for collecting and archiving the radar observations. And authors—we are also acknowledge the State Key Laboratory of Severe Weather, Chinese Academy of Meteorological Sciences & Laboratory of Lightning Physics and Protection Engineering for three-dimensional lightning location data.

## Financial support

- This research has been supported by the National Natural Science Foundation of China (grant nos.
- 42175090 and 42305079), the China Postdoctoral Science Foundation (grant no. 2023M730619),
- the Natural Science Foundation of Sichuan Province (grant no. 2024NSFSC0771), and the Scientific
- 840 Research Fund of Chengdu University of Information Technology (grant nos. KYTZ202213,
- 841 KYQN202301, and KYQN202307).

842

843

#### **Author contributions:**

- Conceptualization: CZ and YZ. Data curation: CZ, YZ, DZ, SD, and WY. Formal analysis: CZ, YZ,
- XP, and YD. Funding acquisition: YZ and CZ. Investigation: CZ, YZ, and XP. Methodology: CZ,
- 846 YZ, HZ, ZL, and DZ. Project administration: YZ. Resources: CZ and YZ. Software: CZ, HZ, and
- 847 ZL. Supervision: YZ. Validation: CZ and YZ. Visualization: CZ and YZ. Writing (original draft):
- 848 CZ, YZ, and XP.

## 849 **Competing interests:**

The contact author has declared that none of the authors has any competing interests.

851

852

- Data and materials availability: All data in this study can be obtained from an open repository
- 853 Figshare (Zhao, 2024).

854

855

## References

- Amiot, C. G., Carey, L. D., Roeder, W. P., McNamara, T. M. and Blakeslee, R. J.: C-band Dual-
- Polarization Radar Signatures of Wet Downbursts around Cape Canaveral, Florida. Weather and Forecasting, 34(1): 103-131, 10.1175/waf-d-18-0081.1, 2019.
- 859 Baker, M. B., Blyth, A. M., Christian, H. J., Latham, J., Miller, K. L. and Gadian, A. M.:
- Relationships between lightning activity and various thundercloud parameters: satellite and
- modelling studies. Atmospheric Research, 51: 221-236, 10.1016/S0169-8095(99)00009-5,
- 862 1999.
- Baker, M. B., Christian, H. J. and Latham, J.: A computational study of the relationships linking
- lightning frequency and other thundercloud parameters. Quarterly Journal of the Royal Meteorological Society, 121(527): 1525-1548, 10.1002/qj.49712152703, 1995.
- Braham, R. R. Jr.: The cloud physics of weather modification. Part 1: Scientific basis. WMO
- Bulletin, 35, 215–221, 1986.

  Rringi, V. N. and Chandrasakar, V.: Polarimetric, Donnler, Weather, Padar: 1
- Bringi, V. N. and Chandrasekar, V.: Polarimetric Doppler Weather Radar: Principles and Applications. Cambridge University Press, Cambridge. 2001.
- Bringi, V. N., Knupp, K., Detwiler, A., Liu, L., Caylor, I. J. and Black, R. A.: Evolution of a Florida
- 871 Thunderstorm during the Convection and Precipitation/Electrification Experiment: The Case

- of 9 August 1991. Monthly Weather Review, 125(9): 2131-2160, https://doi.org/10.1175/1520-0493(1997)125<2131:EOAFTD>2.0.CO;2, 1997.
- 874 Bringi, V. N., Liu, L., Kennedy, P. C., Chandrasekar, V. and Rutledge, S. A.: Dual Multiparameter 875 Radar Observations of Intense Convective Storms: The 24 June 1992 Case Study. Meteorology 876 and Atmospheric Physics, 59: 3-31, 10.1007/BF01031999, 1996.
- 877 Bruning, E. C. and MacGorman, D. R.: Theory and Observations of Controls on Lightning Flash
  878 Size Spectra. Journal of the Atmospheric Sciences, 70(12): 4012-4029, 10.1175/jas-d-12879 0289.1, 2013.
- 880 Bruning, E. C., Brunner, K. N., van Lier-Walqui, M., Logan, T. and Matsui, T.: Lightning and Radar
  881 Measures of Mixed-Phase Updraft Variability in Tracked Storms during the TRACER Field
  882 Campaign in Houston, Texas. Monthly Weather Review, 152, 2753-2769,
  883 https://doi.org/10.1175/MWR-D-24-0060.1, 2024.
- Carey, L. D. and Rutledge, S. A.: A Multiparameter Radar Case Study of the Microphysical and Kinematic Evolution of a Lightning Producing Storm. Meteorology and Atmospheric Physics, 59(1): 33-64, 10.1007/BF01032000, 1996.
- Carey, L. D. and Rutledge, S. A.: The Relationship between Precipitation and Lightning in Tropical Island Convection: A C-Band Polarimetric Radar Study. Monthly Weather Review, 128(8): 2687-2710, 10.1175/1520-0493(2000)128<2687:TRBPAL>2.0.CO;2, 2000.
- 890 Chang, W., Lee, W. and Liou, Y.: The kinematic and microphysical characteristics and associated
  891 precipitation efficiency of subtropical convection during SoWMEX/TiMREX. Monthly
  892 Weather Review, 143(1): 317–340. https://doi.org/10.1175/MWR-D-14-00081.1, 2015.
- Deierling, W. and Petersen, W. A.: Total lightning activity as an indicator of updraft characteristics.

  Journal of Geophysical Research: Atmospheres, 113(D16), 10.1029/2007jd009598, 2008.
- Deierling, W., Petersen, W. A., Latham, J., Ellis, S. and Christian, H. J.: The relationship between lightning activity and ice fluxes in thunderstorms. Journal of Geophysical Research: Atmospheres, 113(D15), 10.1029/2007jd009700, 2008.
- Fan, X. P., Zhang, Y. J., Zheng, D., Zhang, Y., Lyu, W. T., Liu, H. Y. and Xu, L. T.: A New Method of Three-Dimensional Location for Low-Frequency Electric Field Detection Array. Journal of Geophysical Research: Atmospheres, 123(16): 8792-8812, 10.1029/2017jd028249, 2018.
- Fridlind, A. M., van Lier-Walqui, M., Collis, S., Giangrande, S. E., Jackson, R. C., Li, X., Matsui,
   T., Orville, R., Picel, M. H., Rosenfeld, D., Ryzhkov, A., Weitz, R. and Zhang, P.: Use of
   polarimetric radar measurements to constrain simulated convective cell evolution: a pilot study
   with Lagrangian tracking. Atmospheric Measurement Techniques, 12(6): 2979-3000,
   10.5194/amt-12-2979-2019, 2019.
- 906 Gatlin, P. N. and Goodman, S. J.: A Total Lightning Trending Algorithm to Identify Severe 907 Thunderstorms. Journal of Atmospheric and Oceanic Technology, 27(1): 3-22, 10.1175/2009jtecha1286.1, 2010.
- 909 Green, A. W.: An Approximation for the Shapes of Large Raindrops. Journal of Applied
  910 Meteorology and Climatology, 14: 1578-1583, https://doi.org/10.1175/1520911 0450(1975)014<1578:AAFTSO>2.0.CO;2, 1975.
- 912 Gremillion, M. S., and Orville, R. E.: Thunderstorm Characteristics of Cloud-to-Ground Lightning 913 at the Kennedy Space Center, Florida: A Study of Lightning Initiation Signatures as Indicated 914 by the WSR-88D. Weather and Forecasting, 14: 640-649, 1999.
- 915 Goodman, S. J., Blakeslee, R., Christian, H., Koshak, W., Bailey, J., Hall, J., McCaul, E., Buechler,

- D., Darden, C., Burks, J., Bradshaw, T. and Gatlin, P.: The North Alabama Lightning Mapping
- 917 Array: Recent severe storm observations and future prospects. Atmospheric Research, 76(1-4):
- 918 423-437, 10.1016/j.atmosres.2004.11.035, 2005.
- 919 Hayashi, S., Umehara, A., Nagumo, N. and Ushio, T.: The relationship between lightning flash rate
- 920 and ice-related volume derived from dual-polarization radar. Atmospheric Research, 248,
- 921 10.1016/j.atmosres.2020.105166, 2021.
- 922 Helmus, J. J. and Collis, S. M.: The Python ARM Radar Toolkit (Py-ART), a Library for Working
- with Weather Radar Data in the Python Programming Language. Journal of Open Research
- 924 Software, 4(1), 10.5334/jors.119, 2016.
- 925 Herzegh, P. H. and Jameson, A. R.: Observing Precipitation through Dual-Polarization Radar
- 926 Measurements. Bulletin American Meteorological Society, 73(9): 1365-1376, 10.1175/1520-
- 927 0477(1992)073<1365:OPTDPR>2.0.CO;2, 1992.
- 928 Homeyer, C. R. and Kumjian, M. R.: Microphysical Characteristics of Overshooting Convection
- 929 from Polarimetric Radar Observations. Journal of the Atmospheric Sciences, 72(2): 870-891,
- 930 10.1175/jas-d-13-0388.1, 2015.
- 931 Hu, J. and Ryzhkov, A.: Climatology of the Vertical Profiles of Polarimetric Radar Variables and
- 932 Retrieved Microphysical Parameters in Continental/Tropical MCSs and Landfalling
- 933 Hurricanes. Journal of Geophysical Research: Atmospheres, 127(5), 10.1029/2021jd035498,
- 934 2022.
- 935 Hubbert, J., Bringi, V. N., Carey, L. D. and Bolen, S.: CSU-CHILL Polarimetric Radar
- 936 Measurements from a Severe Hail Storm in Eastern Colorado. Journal of Applied Meteorology
- 937 and Climatology, 37(8): 749-775, 10.1175/1520-0450(1998)037<0749:CCPRMF>2.0.CO;2,
- 938 1998.
- 939 Hubbert, J. C., Wilson, J. W., Weckwerth, T. M., Ellis, S. M., Dixon, M. and Loew, E.: S-Pol's
- 940 Polarimetric Data Reveal Detailed Storm Features (and Insect Behavior). Bulletin of the
- 941 American Meteorological Society, 99(10): 2045-2060, 10.1175/bams-d-17-0317.1, 2018.
- 942 Krause, J. and Klaus, V.: Identifying ZDR Columns in Radar Data with the Hotspot Technique.
- 943 Weather and Forecasting, 39(3): 581-595, 10.1175/waf-d-23-0146.1, 2024.
- 944 <u>Kumjian, M. R.: The Impact of Precipitation Physical Processes on the Polarimetric Radar Variables.</u>
- Ph. D. Dissertation, The University of Oklahoma, Norman, OK, USA, 327p., 2012.
- 946 Kumjian, M. R.: Principles and applications of dual-polarization weather radar. Part I: Description
- 947 of the polarimetric radar variables. Journal of Operational Meteorology, 1(19): 226-242,
- 948 10.15191/nwajom.2013.0119, 2013a.
- 949 Kumjian, M. R.: Principles and applications of dual-polarization weather radar. Part II: Warm- and
- 950 cold-season applications. Journal of Operational Meteorology, 1(20): 243-264,
- 951 10.15191/nwajom.2013.0120, 2013b.
- 952 Kumjian, M. R.: Principles and applications of dual-polarization weather radar. Part III: Artifacts.
- 953 Journal of Operational Meteorology, 1(21): 265-274, 10.15191/nwajom.2013.0121, 2013c.
- 954 Kumjian, M. R., Khain, A. P., Benmoshe, N., Ilotoviz, E., Ryzhkov, A. V. and Phillips, V. T. J.: The
- Anatomy and Physics of ZDR Columns: Investigating a Polarimetric Radar Signature with a
- 956 Spectral Bin Microphysical Model. Journal of Applied Meteorology and Climatology, 53(7):
- 957 1820-1843, 10.1175/jamc-d-13-0354.1, 2014.
- 958 Kumjian, M. R., Prat, O. P., Reimel, K. J., van Lier-Walqui, M. and Morrison, H. C.: Dual-
- Polarization Radar Fingerprints of Precipitation Physics: A Review. Remote Sensing, 14, 3706,

- 960 <u>https://doi.org/10.3390/rs14153706, 2022.</u>
- Lang, T. J. and Rutledge, S. A.: A Framework for the Statistical Analysis of Large Radar and
   Lightning Datasets: Results from STEPS 2000. Monthly Weather Review, 139(8): 2536-2551,
   10.1175/mwr-d-10-05000.1, 2011.
- Latham, J. and Dye, J. E.: Calculations on the electrical development of a small thunderstorm.
   Journal of Geophysical Research: Atmospheres, 94(D11): 13141-13144,
   https://doi.org/10.1029/JD094iD11p13141, 1989.
- Li, H., Moisseev, D., Luo, Y., Liu, L., Ruan, Z., Cui, L. and Bao, X.: Assessing specific differential
   phase (KDP)-based quantitative precipitation estimation for the record- breaking rainfall over
   Zhengzhou city on 20 July 2021. Hydrology and Earth System Sciences, 27(5): 1033-1046,
   10.5194/hess-27-1033-2023, 2023.
- Li, H. Q., Wan, Q., Peng, D., Liu, X. and Xiao, H.: Multiscale analysis of a record-breaking heavy
   rainfall event in Guangdong, China. Atmospheric Research, 232: 104703.
   https://doi.org/10.1016/j.atmosres.2019.104703, 2019.
- Li, H., Yin, J. and Kumjian, M.: Z Backwards Arc: Evidence of Multi-Directional Size Sorting in
   the Storm Producing 201.9 mm Hourly Rainfall. Geophysical Research Letters, 51(10):
   e2024GL109192, https://doi.org/10.1029/2024GL109192, 2024.
- Liu, D., Li, F., Qie, X., Sun, Z., Wang, Y., Yuan, S., Sun, C., Zhu, K., Wei, L., Lyu, H. and Jiang, R.:
   Charge Structure and Lightning Discharge in a Thunderstorm Over the Central Tibetan Plateau.
   Geophysical Research Letters, 51(16): e2024GL109602,
   https://doi.org/10.1029/2024GL109602, 2024.
- Liu, Z., Zheng, D., Guo, F., Zhang, Y., Zhang, Y., Wu, C., Chen, H. and Han, S.: Lightning activity
   and its associations with cloud structures in a rainstorm dominated by warm precipitation.
   Atmospheric Research, 246, 10.1016/j.atmosres.2020.105120, 2020.
- Loney, M. L., Zrnić, D. S., Straka, J. M. and Ryzhkov, A. V.: Enhanced Polarimetric Radar Signatures above the Melting Level in a Supercell Storm. Journal of Applied Meteorology, 41(12): 1179-1194, https://doi.org/10.1175/1520-0450(2002)041<1179:EPRSAT>2.0.CO;2, 2002.
- López, R. E. and Aubagnac, J.-P.: The lightning activity of a hailstorm as a function of changes in
   its microphysical characteristics inferred from polarimetric radar observations. Journal of
   Geophysical Research: Atmospheres, 102(D14): 16799-16813,
   https://doi.org/10.1029/97JD00645, 1997.
- 992 Marshall, T. C., Rust, W. D. and Stolzenburg, M.: Electrical structure and updraft speeds in 993 thunderstorms over the southern Great Plains. Journal of Geophysical Research: Atmospheres, 994 100(D1): 1001-1015, https://doi.org/10.1029/94JD02607, 1995.
- 995 Mitzeva, R. and Saunders, C. P. R.: Thunderstorm charging: calculations of the effect of ice crystal 996 size and graupel velocity. Journal of Atmospheric and Terrestrial Physics, 52(4): 241-245, 997 https://doi.org/10.1016/0021-9169(90)90090-A, 1990.
- 998 Mosier, R. M., Schumacher, C., Orville, R. E. and Carey, L. D.: Radar Nowcasting of Cloud-to-999 Ground Lightning over Houston, Texas. Weather and Forecasting, 26(2): 199-212, 1000 https://doi.org/10.1175/2010WAF2222431.1, 2011.
- Park, H. S., Ryzhkov, A. V., Zrnić, D. S., and Kim, K.: The Hydrometeor Classification Algorithm for the Polarimetric WSR-88D: Description and Application to an MCS. Weather and Forecasting, 24: 730-748, https://doi.org/10.1175/2008WAF2222205.1, 2009.

- Pruppacher, H. R., and Klett, J. D.: Microphysics of Clouds and Precipitation. 2d ed. Kluwer Academic, 954 pp., 1997.
- Qie, X., Yu, Y., Liu, X., Guo, C., Wang, D., Watanabe, T. and Ushio, T.: Charge analysis on lightning discharges to the ground in Chinese inland plateau (close to Tibet). Ann. Geophys., 18(10): 1340-1348, 10.1007/s00585-000-1340-z, 2000.
- 1009 Reynolds, S. E., Brook, M. and Gourley, M. F.: THUNDERSTORM CHARGE SEPARATION.
  1010 Journal of Atmospheric Sciences, 14(5): 426-436, https://doi.org/10.1175/15201011 0469(1957)014<0426:TCS>2.0.CO;2, 1957.
- Rison, W., Thomas, R. J., Krehbiel, P. R., Hamlin, T. and Harlin, J.: A GPS-based three-dimensional lightning mapping system: Initial observations in central New Mexico. Geophysical Research Letters, 26(23): 3573-3576, https://doi.org/10.1029/1999GL010856, 1999.
- Rosenfeld, D., Lohmann, U., Raga, G. B., O'Dowd, C. D., Kulmala, M., Fuzzi, S., Reissell, A. and Andreae, M. O.: Flood or Drought: How Do Aerosols Affect Precipitation? Science, 321(5894): 1309-1313, doi:10.1126/science.1160606, 2008.
- 1018 Ryzhkov, A., and Zrnić, D.: Assessment of Rainfall Measurement That Uses Specific Differential
  1019 Phase. Journal of Applied Meteorology and Climatology, 35: 2080-2090,
  1020 https://doi.org/10.1175/1520-0450(1996)035<2080:AORMTU>2.0.CO;2, 1996.
- 1021 Saunders, C.: Charge Separation Mechanisms in Clouds. Space Science Reviews, 137(1): 335-353, 1022 10.1007/s11214-008-9345-0, 2008.
- Seliga, T. A. and Bringi, V. N.: Potential Use of Radar Differential Reflectivity Measurements at
  Orthogonal Polarizations for Measuring Precipitation. Journal of Applied Meteorology and
  Climatology, 15(1): 69-76, https://doi.org/10.1175/15200450(1976)015<0069:PUORDR>2.0.CO;2, 1976.
- Sharma, M., Tanamachi, R. L. and Bruning, E. C.: Investigating Temporal Characteristics of Polarimetric and Electrical Signatures in Three Severe Storms: Insights from the VORTEX-Southeast Field Campaign. Monthly Weather Review, 152(7): 1511-1536, https://doi.org/10.1175/MWR-D-23-0144.1, 2024.
- Sharma, M., Tanamachi, R. L., Bruning, E. C. and Calhoun, K. M.: Polarimetric and Electrical Structure of the 19 May 2013 Edmond–Carney, Oklahoma, Tornadic Supercell. Monthly Weather Review, 149(7): 2049-2078, https://doi.org/10.1175/MWR-D-20-0280.1, 2021.
- Shi, D., Zheng, D., Zhang, Y., Zhang, Y., Huang, Z., Lu, W., Chen, S. and Yan, X.: Low-frequency
  E-field Detection Array (LFEDA)—Construction and preliminary results. Science China Earth
  Sciences, 60(10): 1896-1908, 10.1007/s11430-016-9093-9, 2017.
- Snyder, J. C., Bluestein, H. B., Dawson II, D. T. and Jung, Y.: Simulations of Polarimetric, X-Band Radar Signatures in Supercells. Part I: Description of Experiment and Simulated phy Rings. Journal of Applied Meteorology and Climatology, 56(7): 1977-1999, https://doi.org/10.1175/JAMC-D-16-0138.1, 2017.
- Snyder, J. C., Ryzhkov, A. V., Kumjian, M. R., Khain, A. P. and Picca, J.: A ZDR Column Detection Algorithm to Examine Convective Storm Updrafts. Weather and Forecasting, 30(6): 1819-1844, https://doi.org/10.1175/WAF-D-15-0068.1, 2015.
- Souza, J. C. S. and Bruning, E. C.: Assessment of Turbulence Intensity in Different Spots of Lightning Flash Propagation. Geophysical Research Letters, 48(21): e2021GL095923, https://doi.org/10.1029/2021GL095923, 2021.
- 1047 Straka, J. M., Zrnić, D. S. and Ryzhkov, A. V.: Bulk Hydrometeor Classification and Quantification

- 1048 <u>Using Polarimetric Radar Data: Synthesis of Relations. Journal of Applied Meteorology and</u> 1049 <u>Climatology, 39: 1341-1372, https://doi.org/10.1175/1520-</u> 1050 <u>0450(2000)039<1341:BHCAQU>2.0.CO;2, 2000.</u>
- Takahashi, T.: Riming Electrification as a Charge Generation Mechanism in Thunderstorms. Journal of Atmospheric Sciences, 35(8): 1536-1548, https://doi.org/10.1175/1520-0469(1978)035<1536:REAACG>2.0.CO;2, 1978.
- Tuttle, J. D., Bringi, V. N., Orville, H. D. and Kopp, F. J.: Multiparameter Radar Study of a Microburst: Comparison with Model Results. Journal of Atmospheric Sciences, 46(5): 601-620, https://doi.org/10.1175/1520-0469(1989)046<0601:MRSOAM>2.0.CO;2, 1989.
- van Lier-Walqui, M., Fridlind, A. M., Ackerman, A. S., Collis, S., Helmus, J., MacGorman, D. R.,
   North, K., Kollias, P. and Posselt, D. J.: On Polarimetric Radar Signatures of Deep Convection
   for Model Evaluation: Columns of Specific Differential Phase Observed during MC3E.
   Monthly Weather Review, 144(2): 737-758, https://doi.org/10.1175/MWR-D-15-0100.1, 2016.
- Vincent, B. R., Carey, L. D. Schneider, D., Keeter, K., and Gonski, R.: Using WSR-88D reflectivity
   data for the prediction of cloud-to-ground lightning: A central North Carolina study. Nat. Wea.
   Dig., 27: 35-44, 2003.
- Williams, E., Boldi, B., Matlin, A., Weber, M., Hodanish, S., Sharp, D., Goodman, S., Raghavan, R.
   and Buechler, D.: The behavior of total lightning activity in severe Florida thunderstorms.
   Atmospheric Research, 51(3): 245-265, https://doi.org/10.1016/S0169-8095(99)00011-3,
   1999.
- Williams, E. R., Weber, M. E. and Orville, R. E.: The relationship between lightning type and convective state of thunderclouds. Journal of Geophysical Research: Atmospheres, 94(D11): 13213-13220, https://doi.org/10.1029/JD094iD11p13213, 1989.
- Woodard, C. J., Carey, L. D., Petersen, W. A., and Roeder, W. P.: Operational utility of dualpolarization variables in lightning initiation forecasting, Electronic J. Operational Meteor., 13, 79-102, 2012.
- Yan, M., Guo, C., Ge, Z.: Numerical study of cloud dynamic-electrification in an axisymmetric, time-dependent cloud model. I: Theory and model. ACTA GEOPHYSICA SINICA, 39: 52-64, 1996a.
- Yan, M., Guo, C., Ge, Z.: Numerical study of cloud dynamic-electrification in an axisymmetric, time-dependent cloud model. II: Calculation results. ACTA GEOPHYSICA SINICA, 39: 65-77, 1996b.
- Zhang, Y., Sun, A., Yan, M., Guo, F., Qie, X., Huang, M.: Numerical modeling for effects of electric
   activity during thunderstorms upon the growth of hail particles. Chinese Journal of Geophysics,
   47(1): 25-32, 2004a.
- Zhang, Y., Dong, W., Zhao, Y., Zhang, G., Zhang, H., Chen, C. and Zhang, T.: Study of charge
   structure and radiation characteristic of intracloud discharge in thunderstorms of Qinghai-Tibet
   Plateau. Science in China Series D: Earth Sciences, 47(1): 108-114, 10.1007/BF02880986,
   2004b.
- Zhang, Y., Yan, M., Sun, A., Guo, F.: Thunderstorm Electricity, China Meteorology Press, Beijing,
   384 pp., 2009.
- Zhao, C.: Data for "Bridging the polarimetric structure and lightning activity of an isolated thunderstorm during the cloud life cycle". Figshare. [Dataset]. https://doi.org/10.6084/m9.figshare.28070105.v1, 2024.

- 1092 Zhao, C., Zhang, Y., Zheng, D., Li, H., Du, S., Peng, X., Liu, X., Zhao, P., Zheng, J. and Shi, J.:
- Technical note: On the ice microphysics of isolated thunderstorms and non-thunderstorms in
- southern China a radar polarimetric perspective. Atmospheric Chemistry and Physics, 24(20):
- 1095 11637-11651, 10.5194/acp-24-11637-2024, 2024.
- 2096 Zhao, C., Zhang, Y., Zheng, D., Liu, X., Zhang, Y., Fan, X., Yao, W. and Zhang, W.: Using
- 1097 Polarimetric Radar Observations to Characterize First Echoes of Thunderstorms and
- Nonthunderstorms: A Comparative Study. Journal of Geophysical Research: Atmospheres,
- 1099 127(23): e2022JD036671, https://doi.org/10.1029/2022JD036671, 2022.
- 1100 Zhao, C., Zhang, Y., Zheng, D., Zhou, Y., Xiao, H. and Zhang, X.: An improved hydrometeor
- identification method for X-band dual-polarization radar and its application for one summer
- Hailstorm over Northern China. Atmospheric Research, 245: 105075,
- 1103 https://doi.org/10.1016/j.atmosres.2020.105075, 2020.
- 2104 Zhao, C., Zheng, D., Zhang, Y., Liu, X., Zhang, Y., Yao, W. and Zhang, W.: Turbulence
- 1105 Characteristics of Thunderstorms Before the First Flash in Comparison to Non-Thunderstorms.
- 1106 Geophysical Research Letters, 48(18): e2021GL094821,
- 1107 https://doi.org/10.1029/2021GL094821, 2021a.
- 1108 Zhao, C., Zheng, D., Zhang, Y. J., Liu, X., Zhang, Y., Yao, W., and Zhang, W.: Characteristics of
- 1109 <u>cloud microphysics at positions with flash initiations and channels in convection and stratiform</u>
- 1110 <u>areas of two squall lines, Journal of Tropical Meteorology, 37: 358-369,</u>
- doi:10.16032/j.issn.1004-4965.2021.035, 2021b.
- Zheng, D. and Zhang, Y.: New Insights Into the Correlation Between Lightning Flash Rate and Size
- in Thunderstorms. Geophysical Research Letters, 48(24): e2021GL096085,
- 1114 https://doi.org/10.1029/2021GL096085, 2021.

1120

- 1115 Zrnić, D. S.: Complete Polarimetric and Doppler Measurements with a Single Receiver Radar.
- Journal of Atmospheric and Oceanic Technology, 8: 159-165, https://doi.org/10.1175/1520-
- 1117 <u>0426(1991)008<0159:CPADMW>2.0.CO;2, 1991.</u>
- 2118 Zrnić, D. S.: Three-body scattering produces precipitation signature of special diagnostic value.
- Radio Science, 22(1): 76-86, https://doi.org/10.1029/RS022i001p00076, 1987.